Atmos. Chem. Phys. Discuss., doi:10.5194/acp-2015-989, 2016
Manuscript under review for journal Atmos. Chem. Phys.
Published: 3 February 2016

Atmospheric Chemistry and Physics Discussions

Global combustion sources of organic aerosols: Model comparison with 84 AMS factor analysis data sets

Tsimpidi A.P.[1], Karydis V.A.[1], Pandis S.N.[2, 3]and Lelieveld J.[1, 4]

[1] Max Planck Institute for Chemistry, Mainz, Germany
[2] Department of Chemical Engineering, University of Patras, Patras, Greece
[3] Department of Chemical Engineering, Carnegie Mellon University, Pittsburgh, PA, USA
[4] Energy, Environment and Water Research Center, Cyprus Institute, Nicosia, Cyprus
*Corresponding author e-mail: a.tsimpidi@mpic.de

Atmos. Chem. Phys. Discuss., doi:10.5194/acp-2015-989, 2016
Manuscript under review for journal Atmos. Chem. Phys.
Published: 3 February 2016

Atmospheric Chemistry and Physics Discussions

Abstract

Emissions of organic compounds from biomass, biofuel and fossil fuel combustion strongly influence the global atmospheric aerosol load. Some of the organics are directly released as primary organic aerosol (POA). Most are emitted in the gas phase and undergo chemical transformations (i.e., oxidation by hydroxyl radical) and form secondary organic aerosol (SOA). In this work we use the global chemistry climate model EMAC with a computationally efficient module for the description of organic aerosol (OA) composition and evolution in the atmosphere (ORACLE). The tropospheric burden of open biomass and anthropogenic (fossil and biofuel) combustion particles is estimated to be 0.59 Tg and 0.63 Tg, respectively, accounting for about 30% and 32% of the total tropospheric OA load. About 30% of the open biomass burning and 10% of the anthropogenic combustion aerosols originate from direct particle emissions while the rest is formed in the atmosphere. A comprehensive dataset of aerosol mass spectrometer (AMS) measurements along with factor-analysis results from 84 field campaigns across the Northern Hemisphere are used to evaluate the model results. Both the AMS observations and the model results suggest that over urban areas both POA (25-40%) and SOA (60-75%) contribute substantially to the overall OA mass while further downwind and in rural areas the POA concentrations decrease substantially and SOA dominates (80-85%). EMAC does a reasonable job in reproducing POA and SOA levels during most of the year. However, it tends to underpredict POA and SOA concentrations during winter indicating that the model misses a wintertime source of OA (e.g., residential biofuel use) and a SOA formation pathway (e.g., multiphase oxidation).

1. Introduction

Organic aerosol (OA) is a major contributor to fine particulate matter mass with potentially harmful effects on the environment and human health (Lelieveld et al., 2013; Poschl, 2005), however, its sources are poorly understood (Kanakidou et al., 2005; Turpin et al., 2000; Goldstein and Galbally, 2007; Donahue et al., 2009). OA comprises primary organic aerosol (POA), directly emitted in the particulate phase, and secondary organic aerosol (SOA), formed within the atmosphere from the oxidation of gas-phase precursors. POA is emitted by anthropogenic combustion

Atmos. Chem. Phys. Discuss., doi:10.5194/acp-2015-989, 2016
Manuscript under review for journal Atmos. Chem. Phys.
Published: 3 February 2016

Atmospheric Chemistry and Physics Discussions

processes (i.e., fossil fuels, biofuels) and open biomass burning (i.e., savannas, forests). Anthropogenic combustion emissions of organic carbon (OC) are estimated at 8.9 Tg yr^{-1} (2.4 Tg yr^{-1} from fossil fuel and 6.5 Tg yr^{-1} from biofuel) with an uncertainty range of 5 to 17 Tg yr^{-1} (Bond et al., 2004). OC emissions from open biomass burning are approximately 25 Tg yr^{-1} with an uncertainty range of 13 to 57 Tg yr^{-1}. This uncertainty mainly relates to the emission factors that depend on the fuel burnt and the type of combustion. POA emitted from combustion sources can evaporate rapidly during atmospheric dilution depending on ambient concentrations (Hildemann et al., 1989; Lipsky and Robinson, 2006). The phase partitioning of the emitted POA depends on the volatility distribution of the emissions. This distribution includes low volatility (LVOC; $C^* < 0.32$ μg m^{-3}), semivolatile (SVOC; 0.32 μg m^{-3} < C^* < 320 μg m^{-3}), and intermediate volatility (IVOC; $3.2x10^2$ μg m^{-3} < C^* < $3.2x10^6$ μg m^6) organic compounds. The corresponding emission factors can be measured using dilution samplers and are estimated as a function of the saturation concentration of the emitted organic compounds (Grieshop et al., 2009). Traditional emission inventories (e.g., Bond et al., 2004) account only for a small fraction of the emitted IVOCs since they are based on filter samples collected at aerosol concentrations up to 10^4 μg m^{-3} (Shrivastava et al., 2008; Robinson et al., 2010). The amount of IVOC emissions missing in traditional inventories is estimated to be between 0.25 and 2.8 times POA emissions (Schauer et al., 1999, 2001, 2002).

Organic emissions further downwind mix with background air, resulting in cooling and dilution and altering their gas-particle partitioning. The organic compounds that remain in the gas phase can undergo chemical transformations (i.e., oxidation by hydroxyl radical), become less volatile and may be transferred to the SOA (Donahue et al., 2006). Therefore, in addition to direct emissions of POA, it is important to understand the potential of combustion emissions to contribute to SOA formation. Numerous studies have indicated that SOA usually exceeds POA even in urban environments with substantial primary emissions (Zhang et al., 2007; Jimenez et al., 2009; Subramanian et al., 2007; Stone et al., 2009). However, the overall contribution of combustion emissions to ambient SOA and OA remains uncertain (Chirico et al., 2010; Miracolo et al., 2011; Samy and Zielinska, 2010; Weitkamp et al., 2007; Gentner et al., 2012; Robinson et al., 2007; Bahreini et al., 2012; Gordon et al., 2014). Together with OA mass concentration, its hygroscopic, chemical and optical

Atmos. Chem. Phys. Discuss., doi:10.5194/acp-2015-989, 2016
Manuscript under review for journal Atmos. Chem. Phys.
Published: 3 February 2016

properties continue to change because of chemical processing by gas-phase oxidants (Kanakidou et al., 2005). These changes affect the radiative forcing of OA on climate through both its direct and indirect aerosol effects (McFiggans et al., 2006; Bond et al., 1999; Bond, 2001; Jacobson, 1999; Kirchstetter et al., 2004; Kotchenruther and Hobbs, 1998; Kotchenruther et al., 1999).

Mass spectrometry has been widely used in aerosol analysis because of the universal, sensitive and rapid detection of aerosol components (McKeown et al., 1991; Suess and Prather, 1999). The Aerosol Mass Spectrometer (AMS) (Jayne et al., 2000; Jimenez et al., 2003) has been the most commonly used instrument in the last decade. AMS is capable of quantitatively measuring the OA mass concentrations with high time and size resolution (Allan et al., 2003; Takegawa et al., 2005; Zhang et al., 2005b). Several factor analysis techniques have been employed to provide information about processes and sources of OA. These techniques include principal component analysis (CPCA; Zhang et al., 2005a), multiple component analysis (MCA; Zhang et al., 2007), hierarchical cluster analysis (Marcolli et al., 2006), the Multilinear Engine (ME-2; Lanz et al., 2008), and positive matrix factorization (PMF; Paatero and Tapper, 1994; Paatero, 1997), with the latter being the most commonly used (Lanz et al., 2007; Nemitz et al., 2008; Aiken et al., 2008; Aiken et al., 2009; Ulbrich et al., 2009; DeCarlo et al., 2010; Mohr et al., 2012; Hayes et al., 2013; Crippa et al., 2014; Carbone et al., 2014; Chen et al., 2015).

PMF allows the classification of OA into different types based on different temporal and mass spectral signatures. Two major components often resolved by the analysis of the AMS measurements are hydrocarbon-like organic aerosol (HOA) and oxygenated organic aerosol (OOA) (Zhang et al., 2005c). Biomass burning OA (BBOA), marine-related OA (MOA) and cooking OA (COA) are other OA components that PMF may identify as important components of the observed OA (Zhang et al., 2007; Crippa et al., 2014; Ng et al., 2011). HOA correlates with combustion tracers (e.g., CO, EC, and NO_x) and is considered as a surrogate for fossil fuel combustion POA (Zhang et al., 2005c; Lanz et al., 2007; Aiken et al., 2009; Ulbrich et al., 2009). BBOA correlates with tracers originating from biomass burning (e.g., acetonitrile, levoglucosan, and potassium) and is considered a surrogate of biomass burning POA (Aiken et al., 2010; Ulbrich et al., 2009). OOA has the same temporal pattern as secondary PM components (e.g. sulfate, nitrate) and is considered

Atmos. Chem. Phys. Discuss., doi:10.5194/acp-2015-989, 2016
Manuscript under review for journal Atmos. Chem. Phys.
Published: 3 February 2016

Atmospheric Chemistry and Physics Discussions

as surrogate for SOA (Zhang et al., 2007; Herndon et al., 2008). OOA can include SOA from various precursors, such as anthropogenic and biogenic VOCs, as well as SVOCs and IVOCs from fossil fuel, biofuel and open biomass burning. PMF often classifies OOA into two subtypes that differ in the degree of oxidation: a more oxygenated low-volatility OOA (LV-OOA) and a less oxygenated semivolatile OOA (SV-OOA) (Jimenez et al., 2009). Field campaigns in the North Hemisphere have shown that HOA accounts for approximately one third of the OA in urban sites while OOA accounts for the remaining two thirds. OOA represents roughly 95% of the OA in rural/remote regions (Zhang et al., 2007).

Global chemistry climate and chemical transport models systematically underpredict OA levels (Heald et al., 2005; de Gouw et al., 2005), especially during episodes of intense photochemistry (Vutukuru et al., 2006; Volkamer et al., 2006). At the same time, traditional global models tend to predict a dominance of POA at mid-latitudes in the Northern Hemisphere while measurements indicate the opposite (Heald et al., 2005; Henze et al., 2008; Tsigaridis et al., 2014). The same models predict that formation of SOA from biogenic sources greatly exceeds that from anthropogenic sources. The shortcomings in the traditional OA models are partially due to the assumption that POA is non-volatile and nonreactive (Kanakidou et al., 2005; Jimenez et al., 2009)). In order to help remedy these shortcomings, Donahue et al. (2006) developed the volatility basis set (VBS) framework which assumes that POA emissions are semivolatile and photochemically reactive and are distributed in logarithmically spaced volatility bins. Recently, several regional-scale modeling studies have accounted for the semivolatile nature and chemical aging of organic compounds demonstrating improvements in reproducing the OA concentrations and its composition (Robinson et al., 2007; Shrivastava et al., 2008; Murphy and Pandis, 2009; Tsimpidi et al., 2010; Tsimpidi et al., 2011; Hodzic et al., 2010; Fountoukis et al., 2011; Bergstrom et al., 2012; Athanasopoulou et al., 2013; Zhang et al., 2013; Fountoukis et al., 2014). However, only few global modeling studies have yet adopted the VBS approach to simulate the SOA formation from the chemical aging of SVOC and IVOC emissions (Pye and Seinfeld, 2010; Jathar et al., 2011; Tsimpidi et al., 2014). The model results indicate a larger share for anthropogenic SOA on a global scale. According to these studies, the modeled tropospheric burden of POA is 0.03-

Atmos. Chem. Phys. Discuss., doi:10.5194/acp-2015-989, 2016
Manuscript under review for journal Atmos. Chem. Phys.
Published: 3 February 2016

0.23 Tg and of SOA 1.6-2.8 Tg, with SVOCs and IVOCs contributing 0.7-1.6 Tg to the total SOA.

In this work we use ORACLE, a computationally efficient module for the description of organic aerosol composition and evolution in the atmosphere (Tsimpidi et al., 2014), to estimate the impact of open biomass burning and anthropogenic combustion emissions and their chemical aging on global OA budgets and distributions. An extensive global dataset of AMS measurements and factor-analysis results from 84 field campaigns in the Northern Hemisphere are used in combination with the model results during the period of 2001-2010. This integrated effort provides further insights into the temporal and geographical variability of the contribution of the emitted particles and the chemically processed organic material from combustion sources to the total OA load.

2. Model description and application

2.1 EMAC Model

The ECHAM/MESSy Atmospheric Chemistry (EMAC) model is a numerical chemistry and climate simulation system that includes sub-models describing the lower and middle atmosphere processes (Jöckel et al., 2006). EMAC includes submodels that describe gas-phase chemistry (MECCA; Sander et al., 2011), inorganic aerosol microphysics (GMXe; Pringle et al., 2010), cloud microphysics (CLOUD; Jöckel et al., 2006), aerosol optical properties (AEROPT; Lauer et al., 2007), dry deposition (DRYDEP; Kerkweg et al., 2006a), sedimentation (SEDI; Kerkweg et al., 2006a), emissions (ONLEM and OFFLEM; Kerkweg et al., 2006b), and organic aerosol formation and growth (ORACLE; Tsimpidi et al., 2014). The spectral resolution used in this study is T63L31, corresponding to a horizontal grid resolution of 1.875^{o}x1.875^{o} and 31 vertical layers extending to 10 hPa at about 25 km altitude. EMAC is applied for 11 years, covering the period 2000–2010, and the first year is used as spin-up.

2.2 ORACLE Module

ORACLE is a computationally efficient submodel for the description of OA composition and evolution in the atmosphere which has been implemented into the

Atmos. Chem. Phys. Discuss., doi:10.5194/acp-2015-989, 2016
Manuscript under review for journal Atmos. Chem. Phys.
Published: 3 February 2016

Atmospheric Chemistry and Physics Discussions

EMAC model by Tsimpidi et al. (2014). ORACLE simulates a variety of semivolatile organic species and reaction products and separates them into groups of compounds with logarithmically spaced effective saturation concentrations.

In this study, primary organic emissions from open biomass burning and from anthropogenic sources (i.e., fossil fuel and biofuel) are simulated using separate surrogate species for each source category. They are subdivided into three groups of organic compounds: low volatility, LVOCs (10^{-2} μg m^{-3}), semi-volatile, SVOCs (10^{0} and 10^{2} μg m^{-3}) and intermediate volatility organic compounds, IVOCs (10^{4} and 10^{6} μg m^{-3}). These organic compounds are allowed to partition between the gas and aerosol phases resulting in the formation of fPOA (anthropogenic POA from fossil fuel and biofuel combustion) and bbPOA (natural POA from open biomass burning). VOCs are distinguished into anthropogenic and biogenic and their oxidation products are distributed in four volatility bins with effective saturation concentrations of 10^{0}, 10^{1}, 10^{2}, and 10^{3} μg m^{-3} at 298 K. Gas-phase photochemical reactions that change the volatility of the organics are taken into account and their oxidation products (SOA-sv, SOA-iv, and SOA-v) are simulated separately in the module to keep track of their origin. The suffixes –sv, -iv and -v after the term SOA declare the group of its precursors (SVOCs, IVOCs, and VOCs, respectively). For the current application, SOA components are divided in four groups based on their source: anthropogenic from fossil fuel and biofuel combustion sources (fSOA), natural from open biomass burning (bbSOA), SOA from anthropogenic (aSOA-v) and biogenic (bSOA-v) VOCs. This study focuses on the OA produced from primary combustion sources and discusses in detail results for the first two types of SOA (fSOA and bbSOA). The model set up for simulating the formation of aSOA-v and bSOA-v and the corresponding results can be found in Tsimpidi et al. (2014). In addition, in this work ORACLE has been modified to distinguish the formation of fresh SOA and aged SOA by adding additional tracers into the model. The first generation oxidation products of SVOCs, IVOCs, and VOCs are characterized as fresh while SOA produced from any additional oxidation step is grouped together and considered aged (Figure 1). LVOCs are not allowed to participate in photochemical reactions since they are in the lowest volatility bin. This assumption may introduce a small bias on our results only under extremely clean conditions (OA $\leq 10^{-2}$ μg m^{-3}) where part of LVOC is in the gas phase. Adding another bin in the volatility distribution to accurately represent the extremely low volatility

Atmos. Chem. Phys. Discuss., doi:10.5194/acp-2015-989, 2016
Manuscript under review for journal Atmos. Chem. Phys.
Published: 3 February 2016

Atmospheric Chemistry and Physics Discussions

organic compounds (e.g., ELVOCs with C^* lower than 10^{-3}) would be useful only for studying new particle formation, which is outside the scope of the current work. The volatilities of SVOCs and IVOCs are reduced by a factor of 10^2 as a result of the OH reaction with a rate constant of 2×10^{-11} cm^3 $molecule^{-1}$ s^{-1} and a 15% increase in mass is assumed to account for two added oxygen atoms (Tsimpidi et al., 2014). While this representation is common for global models (e.g., Pye and Seinfeld, 2010; Tsimpidi et al., 2014), regional models use a more conservative formulation to represent the aging of SVOC and IVOC by assuming a reduction in volatility by one order of magnitude after each oxidation step (e.g., Tsimpidi et al., 2010; Bergstrom et al., 2012). However, the oxidation products can be up to four orders of magnitude lower in volatility than the precursor (Kroll and Seinfeld, 2008). Furthermore, ORACLE calculates the fraction of the semivolatile organic compounds that condenses to (or evaporates from) the particle phase by assuming bulk equilibrium and that all organic compounds form a pseudo-ideal solution (Tsimpidi et al., 2014). Overall, the primary aerosol formation from the phase partitioning of the freshly emitted LVOCs and SVOCs, as well as the formation of SOA from the photo-oxidation of SVOCs and IVOCs are described by the following reactions:

$$LVOC_i \leftrightarrow POA_i \quad \text{(R1)}$$

$$SVOC_i \leftrightarrow POA_i \quad \text{(R2)}$$

$$SVOC_i + OH \rightarrow 1.15\ SOG\text{-}sv_{i-1} \quad \text{(R3)}$$

$$SOG\text{-}sv_i + OH \rightarrow 1.15\ SOG\text{-}sv_{i-1} \quad \text{(R4)}$$

$$SOG\text{-}sv_i \leftrightarrow SOA\text{-}sv_i \quad \text{(R5)}$$

$$IVOC_i + OH \rightarrow 1.15\ SOG\text{-}iv_{i-1} \quad \text{(R6)}$$

$$SOG\text{-}iv_i + OH \rightarrow 1.15\ SOG\text{-}iv_{i-1} \quad \text{(R7)}$$

$$SOG\text{-}iv_i \leftrightarrow SOA\text{-}iv_i \quad \text{(R8)}$$

where *i* is the original volatility bin and *i*-1 is the volatility bin with saturation concentration reduced by a factor of 10^2. The term SOG corresponds to secondary organic gas that is produced by at least one chemical reaction in the atmosphere. The symbol "↔" denotes the equillibrium between the gas and the aerosol phases. It is

Atmos. Chem. Phys. Discuss., doi:10.5194/acp-2015-989, 2016
Manuscript under review for journal Atmos. Chem. Phys.
Published: 3 February 2016

Atmospheric Chemistry and Physics Discussions

worth mentioned that the production of RO_2 as an intermediate after the oxidation of SVOC and IVOC has been omitted since it would be essential only in cases where these reactions are a potentially significant sink of OH (i.e. in concentrated smoke plumes) (Alvarado et al., 2015). The model set-up and the different aerosol types and chemical processes that are simulated by ORACLE for this study are illustrated in Figure 1. More details about ORACLE can be found in Tsimpidi et al. (2014).

2.3 Emission inventory

The CMIP5 RCP4.5 emission inventory (Clarke et al., 2007) is used for the anthropogenic POA emissions from fossil fuel and biofuel combustion sources. The open biomass burning emissions from savanna burning and forest fires are based on the Global Fire Emissions Database (GFED v3.1; van der Werf et al., 2010). These emission datasets report the mass of the OC emitted. Therefore, in order to determine the total organic matter (OM) emitted (including any additional species associated with the carbon) OM/OC values of 1.3 for anthropogenic POA and 1.6 for open biomass burning POA are used. These values are based on the OM/OC values estimated by Aiken et al. (2008) for HOA and BBOA respectively. Furthermore, the above emission datasets are monthly resolved and treat POA as non-reactive and non-volatile. However, only a fraction of this organic material is directly emitted in the aerosol phase as POA. Most of it is rapidly transferred to the gas phase where it can undergo chemical transformations and form SOA. Therefore, a key input for the accurate description of these compounds and their chemical aging is their volatility distribution at 298 K. Figure 2 depicts the volatility distributions assumed for this study which cover a range of volatilities from 10^{-2} to 10^{4} μg m^{-3} for open biomass burning (May et al., 2013) and 10^{-2} to 10^{6} μg m^{-3} for fossil and biofuel combustion emissions (Robinson et al., 2007). Emission inventories are based on samples collected at aerosol concentrations up to 10^{4} μg m^{-3} (Shrivastava et al., 2008; Robinson et al., 2010). As a result IVOC emissions with $C^* > 10^{4}$ μg m^{-3} are missing from the traditional emission inventories and have to be accounted for by assigning additional emissions in this volatility range. We assume that the missing IVOC emissions from anthropogenic combustion are 1.5 times the traditional OA emissions included in the inventory (Shrivastava et al., 2008; Tsimpidi et al., 2010), therefore the sum of the emission factors is 2.5. No IVOC emissions are added for open

Atmos. Chem. Phys. Discuss., doi:10.5194/acp-2015-989, 2016
Manuscript under review for journal Atmos. Chem. Phys.
Published: 3 February 2016

biomass burning and therefore the sum for the biomass burning emission factors is unity. The sensitivity of our results to these assumptions will be discussed in a subsequent article in preparation. Overall, the decadal average global emission flux of SVOCs and IVOCs is 44 Tg yr^{-1} from anthropogenic combustion sources and 28 Tg yr^{-1} from open biomass burning sources.

3. Model evaluation methodology

3.1 Factor analysis of AMS measurements

During the period 2001-2010, 84 field campaigns were performed in the Northern Hemisphere using the AMS for measuring ambient OA concentrations in urban, urban-downwind, and rural environments (Figure 3). Information for each of these campaigns is given in Tables S1-S3. The OA source apportionment for all sites was taken from the literature (Tables S1-S3) and performed using factor-analysis techniques classifying OA as HOA, corresponding roughly to POA from fossil fuel combustion, and OOA, corresponding to SOA. Therefore, AMS HOA is compared with modeled fPOA, which is emitted and remains in the aerosol phase without undergoing any chemical reactions, and AMS-OOA is compared with modeled SOA (the sum of SOA-sv, SOA-iv, and SOA-v), formed from the oxidation of gas phase precursors (SVOCs, IVOCs, and VOCs). At many locations, PMF and other factor analysis techniques identified two subtypes of OOA that differ in volatility and oxidation state: semi-volatile OOA (SV-OOA) and low-volatility OOA (LV-OOA). There are different potential interpretations of SV-OOA and LV-OOA. SV-OOA often correlated with semivolatile species such as ammonium nitrate and was less oxygenated, consistent with relatively fresh SOA (Zhang et al., 2011; Ng et al., 2011). LV-OOA was usually correlated with nonvolatile secondary species such as sulfate and was highly oxygenated, consistent with regional aged OA (Zhang et al., 2011; Ng et al., 2011). Recently, Ehn et al. (2014) found a direct pathway which leads to the formation of fresh LV-OOA from the oxidation of several biogenic VOCs. Here we test the hypothesis that SV-OOA corresponds to the first generation products while LV-OOA to the later generation ones. Therefore, AMS SV-OOA is compared with the fraction of SOA-sv, SOA-iv, and SOA-v from the first oxidation step of SVOCs,

Atmos. Chem. Phys. Discuss., doi:10.5194/acp-2015-989, 2016
Manuscript under review for journal Atmos. Chem. Phys.
Published: 3 February 2016

Atmospheric Chemistry and Physics Discussions

IVOC, and VOCs as it is tracked separately (henceforth EMAC fresh SOA). Then AMS LV-OOA is compared with the fraction of SOA-sv, SOA-iv, and SOA-v from any additional oxidation step (henceforth EMAC aged SOA). Finally, in a few of the field campaigns, e.g., in the Alps (Lanz et al., 2010), residential wood burning was found to be a major source of OA. However, residential wood burning is included in EMAC as fPOA. To account for this inconsistency for the AMS data sets that include BBOA we compare the sum of the simulated fPOA and bbPOA (henceforth EMAC POA) against the sum of the AMS HOA and BBOA (henceforth AMS POA).

3.2 Evaluation metrics

The mean bias (MB), mean absolute gross error (MAGE), normalized mean bias (NMB), normalized mean error (NME), and the root mean square error (RMSE) are used to assess the model performance:

$$MAGE = \frac{1}{N}\sum_{i=1}^{N}\left|P_i - O_i\right| \quad (1) \qquad MB = \frac{1}{N}\sum_{i=1}^{N}\left(P_i - O_i\right) \quad (2)$$

$$NME = \frac{\sum_{i=1}^{N}\left|P_i - O_i\right|}{\sum_{i=1}^{N} O_i} \quad (3) \qquad NMB = \frac{\sum_{i=1}^{N}\left(P_i - O_i\right)}{\sum_{i=1}^{N} O_i} \quad (4)$$

$$RMSE = \left[\frac{1}{N}\sum_{i=1}^{N}\left(P_i - O_i\right)^2\right]^{\frac{1}{2}} \quad (5)$$

where O_i is the observed campaign average value of the ith OA component, P_i is the corresponding modelled value during the same period, and N is the total number of comparisons used for the evaluation. NME (in %) and MAGE (in μg m^{-3}) provide an estimate of the overall discrepancy between predictions and observations, while NMB (in %) and MB (in μg m^{-3}) are sensitive to systematic errors. RMSE (in μg m^{-3}) is the root of the mean square error, which incorporates both the variance of the prediction and its bias. Both NME and MAGE inherently include the corresponding bias, which is the reason why their magnitude is equal or larger than NMB and MB respectively. For an unbiased prediction, NME and MAGE express the variance. When NME and NMB or MAGE and MB are close, the discrepancy is explained as a systematic bias

Atmos. Chem. Phys. Discuss., doi:10.5194/acp-2015-989, 2016
Manuscript under review for journal Atmos. Chem. Phys.
Published: 3 February 2016

Atmospheric Chemistry and Physics Discussions

rather than scatter. When the magnitude of NME/MAGE is larger than NMB/MB, part of the discrepancy between predictions and observations is explained as scatter. In order to determine the effect that the site type or the seasonal cycle has on the performance of the model, the evaluation metrics are calculated separately for urban, urban-downwind, and rural sites and for the four seasons of the year (winter, spring, summer, and autumn).

4. Model results

4.1 OA from anthropogenic combustion

4.1.1 Geographical distribution

Figure 4 depicts the simulated, decadal average global surface concentrations of fPOA and fSOA from anthropogenic SVOC and IVOC sources (fossil and biofuel combustion). The average surface concentration of fPOA is 0.1 μg m^{-3}. Higher fPOA concentrations (up to 14 μg m^{-3}) are simulated over densely populated and highly industrialized areas (e.g., Eastern China, Northern India, Central Europe, etc.) where there are substantial anthropogenic combustion emissions. Further downwind, fPOA concentrations decrease substantially since they are diluted and a large fraction is predicted to evaporate during transport. This results in a highly inhomogeneous spatial distribution of fPOA concentrations (Figure 4a). In contrast, fSOA is more regionally distributed with high concentrations (up to 9.5 μg m^{-3}) downwind of the anthropogenic sources due to its continuous production and long-range transport from SVOCs and IVOCs (Figure 4b). This results in a continental fSOA background of 0.5-1 μg m^{-3} and in concentrations of around 1 μg m^{-3} over marine regions close to anthropogenic sources (e.g., Arabian Sea, Yellow Sea, etc.). The average surface concentration of fSOA is 0.26 μg m^{-3} with 73% of it originating from the oxidation of IVOC emissions. This result supports the hypothesis of several recent studies that IVOC emission and oxidation may be a significant SOA source that is missing from chemistry climate models (Jathar et al., 2011; Tsimpidi et al., 2014). The relatively small contribution (25%) of SVOCs to total fSOA can be justified by its low emissions compared to the IVOCs (two times lower) and by the fact that a significant

Atmos. Chem. Phys. Discuss., doi:10.5194/acp-2015-989, 2016
Manuscript under review for journal Atmos. Chem. Phys.
Published: 3 February 2016

fraction of SVOCs stays in the aerosol phase (as POA) without undergoing any chemical reactions (Tsimpidi et al., 2014).

The fraction of fossil and biofuel combustion OA (fOA) that is formed through the oxidation of gas phase species, fSOA/fOA, is consistently high with values ranging from around 20% close to the sources to 100% away from them with a global average of 83% at surface (Figure 5a). This result suggests that over urban areas both fPOA and fSOA contribute significantly to the overall OA mass while further downwind and in rural areas the SOA formation dominates since POA concentrations decrease substantially due to dilution and evaporation. The OA due to anthropogenic combustion sources contributes significantly to total OA over the continents in the northern Hemisphere (Figure 5b). The highest contribution is predicted over Eastern China (83%) and the lowest over the Southeast US (23%). Over mid-latitude oceans, the contribution of fOA to total OA is also high (around 60%) due to the long-range transport of secondary OA. On the other hand, fOA/OA is very low (0-10%) over the tropical and boreal forest regions due to the significant bbOA and bSOA-v concentrations over these areas. Overall, the predicted global average fOA/OA is 38%. This result highlights the importance of anthropogenic emissions for global OA levels, also suggested by other recent studies (Carslaw et al., 2013; Lee et al., 2013; Spracklen et al., 2011).

4.1.2 Temporal profile

Table 1 shows the decadal average tropospheric burden of fPOA and fSOA. The decadal average tropospheric burden of total fOA is 0.63 Tg (10% fPOA and 90% fSOA). The tropospheric fSOA/fOA is higher than at the surface since SVOC and IVOC continue forming fSOA at higher altitudes (Tsimpidi et al., 2014).

The lower temperatures that occur during winter in the Northern Hemisphere drive the gas-particle partitioning of freshly emitted SVOCs to the aerosol phase resulting in higher fPOA concentrations. The wintertime burden of fPOA is 36% higher than its annual average value (Figure 6a). In the same time, less SVOCs are available in the gas phase to react with the lower wintertime OH resulting in reduced formation of fSOA. The wintertime tropospheric burden of fSOA is 16% lower than its annual average value (Figure 6a) representing 87% of the fOA. During summer, the photooxidation of SVOC and IVOC is significantly enhanced; however, the increase

Atmos. Chem. Phys. Discuss., doi:10.5194/acp-2015-989, 2016
Manuscript under review for journal Atmos. Chem. Phys.
Published: 3 February 2016

in fSOA mass is compensated by evaporation due to the high temperatures resulting in an overall increase of only 3% compared to the annual average values. High temperatures during summer also result in a significant decrease of fPOA due to evaporation, i.e., a 27% decrease compared to the annual average tropospheric burden (Figure 6a). Overall, the tropospheric fSOA:fOA during summer is increased to 93%. The highest fSOA concentrations are predicted during spring (i.e., April) when the photochemistry is enhanced and the moderate temperatures favor the partitioning into the aerosol phase (Figure 6a).

Figure 6b depicts the change of fOA annual tropospheric burden over the simulated years (2001 to 2010). The decadal variability of the model predictions for fOA is very low (±4%) since anthropogenic emissions are assumed to have small differences between the simulated years (Clarke et al., 2007). The anthropogenic SVOC and IVOC emissions from fossil and biofuel combustion increased approximately 0.5 Tg yr^{-1} on average during the simulated decade. The lowest fOA tropospheric burden is calculated during the years 2001 and 2003 (0.61 Tg yr^{-1}) and the highest during the year 2009 (0.66 Tg yr^{-1}).

4.2 OA from open biomass burning

4.2.1 Geographical distribution

Figure 7 depicts the simulated decadal average global surface concentrations of bbPOA and bbSOA. The average surface concentration of bbPOA is 0.11 μg m^{-3}. The highest bbPOA concentrations (up to 7.7 μg m^{-3}) are predicted over the tropical rainforests (i.e., Amazon, Congo, and Southeast Asia) and the boreal forests (i.e., Alaska, Canada, and Russia) due to substantial emissions from forest and savannah fires. Similar to fPOA, bbPOA levels rapidly decrease as the air mass moves away from the source due to dilution and evaporation (Figure 7a). The average surface concentration of bbSOA is 0.15 μg m^{-3}. In contrast to anthropogenic combustion emissions, IVOCs are assumed to account for only 40% of the total open biomass burning emissions. Nevertheless, the model predicts that the bbSOA formed due to the oxidation of IVOCs (46%) is similar to that from the oxidation of SVOCs (54%). This result corroborates our finding that IVOCs are a significant source of SOA. bbSOA concentrations are more spatially homogeneous compared to bbPOA reaching

Atmos. Chem. Phys. Discuss., doi:10.5194/acp-2015-989, 2016
Manuscript under review for journal Atmos. Chem. Phys.
Published: 3 February 2016

high levels (up to 6.4 μg m^{-3}) over a wide area covering most of South America, Central and South Africa, Southeastern Asia, and Indonesia (Figure 7b). The atmosphere over the Southern Atlantic Ocean is also strongly influenced by long-range transport of bbSOA from the Congo Basin (1-3 μg m^{-3}). Over these areas, the atmospheric conditions are favorable for the photochemical oxidation of SVOCs and IVOCs. On the other hand, over the boreal forests, the low temperatures favor the partitioning of SVOCs into the particulate phase forming bbPOA and at the same time the photo-oxidation of IVOCs is slow. This results in moderate average bbSOA concentrations around 0.5 μg m^{-3}.

Figure 8a depicts the predicted decadal average contribution of bbSOA to total bbOA (bbSOA/bbOA) at the surface. bbSOA/bbOA is high with values ranging from around 35% over the large tropical and boreal forests to 85% in areas downwind of them and over the oceans. The global average bbSOA/bbOA at the surface is prediced to be 72%. This result indicates that even though the biomass burning emissions are distributed in relatively low volatility bins ($C^* \leq 10^4$ μg m^{-3}), bbSOA still exceeds primary biomass burning OA on a global scale. Figure 8b depicts the decadal average surface contribution of bbOA to total OA (bbOA/OA). As expected, bbOA contributes significantly to total OA over the tropical and boreal forests (around 60%) while it has a smaller impact on OA levels over the mid-latitude continents of the Northern Hemisphere. This result does not include other types of biomass combustion (e.g., for residential heating) that often contribute significantly over urban areas (Chen et al., 2007; Wang et al., 2007; Lanz et al., 2010). High bbOA contributions are also predicted downwind of the boreal forests (up to 80%). Furthermore, the bbOA/OA ratio is high (50-90%) off the subtropical west coasts of Africa, South America and Indonesia. These high values are due to the chemical aging of biomass burning SVOCs and IVOCs in contrast to the chemical products of biogenic VOCs which are assumed to have very low later generation SOA (Tsimpidi et al., 2014). Overall, the global average bbOA/OA is predicted to be 26%.

4.2.2 Temporal evolution

The decadal average tropospheric burden of total bbOA is 0.59 Tg yr^{-1} (30% bbPOA, 70% bbSOA) (Table 1). The fraction of bbOA that is secondary is less than that of fOA (90%).

Atmos. Chem. Phys. Discuss., doi:10.5194/acp-2015-989, 2016
Manuscript under review for journal Atmos. Chem. Phys.
Published: 3 February 2016

466 The interannual variability of bbPOA and bbSOA is high due to the seasonal
467 variability of fires (Figure 9a). During the months of July to September (dry season),
468 intense wildfires are reported over the tropics related to the low precipitation and high
469 temperatures. This results in high biomass burning emissions which together with the
470 intense photochemical activity result in bbOA tropospheric burdens of up to 1.4 Tg
471 yr^{-1} during August (130% higher than the annual average). The lowest bbOA
472 tropospheric burdens are estimated during the wet season (0.21 Tg yr^{-1} during April,
473 64% lower than the annual average). Furthermore, during the dry season OA consists
474 mainly of bbOA over the tropical rainforests due to the intense wildfires while during
475 the wet season OA consists mainly of biogenic SOA since biomass burning emissions
476 are low. As a result, the bbOA/OA has a significant seasonal variability as well;
477 during the dry season the global average bbOA/OA increases significantly (e.g., 41%
478 during August; not shown) while during the wet season it is significantly lower (e.g.,
479 11% during March; not shown).
480 The decadal variability of the model predictions is also important since open
481 biomass burning emissions can vary significantly from year to year (Figure 9b). The
482 years 2001 and 2009 had low fire emissions and the bbOA annual tropospheric
483 burden was 0.47 Tg yr^{-1} (21% lower than the decadal average). The year of 2010 on
484 the other hand was characterized by severe wildfires, especially over the Amazon
485 region resulting in a bbOA annual tropospheric burden of 0.72 Tg yr^{-1} (21% higher
486 than the decadal average). This is consistent with Chen et al. (2013) who analyzed
487 satellite data to detect the fire activity over the Amazon rainforest and reported a
488 twofold increase in fire activity during 2010 compared to 2009.
489
490 **5. Comparison with AMS data**
491
492 **5.1 Spatial evaluation**
493
494 **5.1.1 POA**
495 AMS observations indicate that over urban areas POA (the sum of HOA and
496 BBOA) has relatively high concentrations while further downwind and in rural areas
497 it decreases substantially due to dilution and evaporation (Figure 10a). The model
498 significantly underpredicts (NMB=-65%, Table 2) the high values of POA over urban

Atmos. Chem. Phys. Discuss., doi:10.5194/acp-2015-989, 2016
Manuscript under review for journal Atmos. Chem. Phys.
Published: 3 February 2016

areas and especially over densely populated areas such as Beijing, Tokyo and Mexico City (Table S1). However, this underprediction is partly associated with the limited spatial resolution of the model since the size of the grid cell used typically exceeds the size of most urban centers. The model does a better job in reproducing the measured POA values over urban-downwind locations. This can be verified by focusing on specific field campaigns that provide data from both the urban center and urban-downwind locations over the same period of time (i.e., MILAGRO over Mexico City and MEGAPOLI over Paris). Over these areas the model captures the measured POA concentrations downwind of the urban center (Table S2) but it significantly underpredicts the POA concentrations measured in the urban center (Table S1). Overall, over urban-downwind and rural areas the model captures the low values of POA (Figure 10a). Over urban-downwind areas, the model slightly underpredicts POA (NMB=-15%) while over rural areas it overpredicts by 0.04 μg m^{-3} (Table 2). However, over rural areas with high BBOA concentrations (e.g, Massognex, Payerne, etc.) the model underpredicts POA (Table S3) indicating that biomass burning sources over residential areas may be underestimated in the emission inventory. The possible underestimation of biomass burning emissions over European residential areas has been recently reported by several studies (Bergstrom et al., 2012; Kostenidou et al., 2013; Denier van der Gon et al., 2014).

5.1.2 SOA

Both AMS and EMAC model results indicate that SOA (or OOA) is high over all types of environments (Table 3). The highest concentrations are found over urban locations (AMS-OOA= 4.33 μg m^{-3} and EMAC-SOA= 2.97 μg m^{-3}) while further downwind SOA concentrations decrease by 37% over rural locations according to both AMS and EMAC results (Figure 10b). This indicates that the initial emissions of VOCs, IVOCs and SVOCs are photo-oxidized rapidly in the urban environment producing SOA, while their atmospheric aging and further production of SOA is offset by dilution as the air mass moves away from the urban center. EMAC does a reasonable job in reproducing SOA concentrations (Table 3), however, an underprediction is found in all types of environments. The best model performance is achieved over urban downwind locations (NMB=-25%) followed by urban and rural areas (NMB=-31% and -32%, respectively). Similar to POA, the model underpredicts

Atmos. Chem. Phys. Discuss., doi:10.5194/acp-2015-989, 2016
Manuscript under review for journal Atmos. Chem. Phys.
Published: 3 February 2016

SOA over densely populated areas such as Beijing and Mexico City (Table S1) due to its limited spatial resolution. In addition, the model significantly underpredicts SOA over specific urban-downwind and rural areas. In most of these cases the field campaign was short (up to 1 week) and the results were subject to specific pollution episodes which cannot be captured by our model (e.g., Puy de Dome, Table S3).

In most of the available datasets (51 out of 84), PMF provides information for the two subtypes of OOA (LV-OOA and SV-OOA). Both PMF and EMAC results indicate that aged SOA (or LV-OOA) is higher than fresh SOA (or SV-OOA) regardless of the type of environment. The EMAC performance is better over urban locations where it reproduces the high levels of aged SOA with NMB=-21% and NME=43% (Table 4). Over urban-downwind and rural locations EMAC underpredicts aged SOA with NMB=-47% and -38%, respectively (Table 4). The performance of the model for fresh SOA is better compared to aged SOA (Table 4) indicating that the modeled OA aging parameterization may underestimate the SOA produced from atmospheric aging and requires improvements. Similar to aged SOA, the best performance of the model for fresh SOA is obtained over urban locations (NMB=-12%).

5.2 Seasonal evaluation

The seasonal model performance evaluation does not include the values over the urban areas because most of the corresponding field campaigns were conducted during winter and summer. In parallel, as discussed above, the model cannot reproduce the concentrations of POA and SOA over urban locations due to its coarse resolution. Therefore including urban locations in our analysis will bias the model performance during winter and summer leading to a potential misinterpretation of the corresponding results regarding the seasonal performance of the model.

5.2.1 POA

The model performs best during summer (RMSE=0.4, NMB=-3%), followed by autumn (RMSE=0.37, NMB=-15%) and spring (RMSE=0.52, NMB=21%). During winter EMAC underpredicts POA with NMB=-34% (Table 2; Figure 11a). This result corroborates our hypothesis that residential biofuel emissions may be underestimated in the inventory since most of the residential heating occurs during winter.

Atmos. Chem. Phys. Discuss., doi:10.5194/acp-2015-989, 2016
Manuscript under review for journal Atmos. Chem. Phys.
Published: 3 February 2016

Atmospheric Chemistry and Physics Discussions

Furthermore, since vehicle catalysts require a certain temperature to work to full efficiency, emissions from gasoline and diesel vehicles are significantly higher during the warm-up phase of the car (Westerholm et al., 1996). Typically, the additional emissions during the warm-up phase (or cold-start emissions) are accounted in emission inventories based on measurements at an ambient temperature of 23 ^{o}C (Weilenmann et al., 2009). However, cold-start emissions increase considerably at lower ambient temperatures varying by more than one order of magnitude between 23 and -20 ^{o}C (Weilenmann et al., 2009) and thus significant underestimations of OA emissions from the transport sector can be expected during wintertime. Kopacz et al. (2010) provide a global estimate of CO sources by adjoint inversion of satellite datasets and reported an underestimation of CO sources during the winter season due to larger than expected CO emissions from vehicle cold starts and residential heating. Another source of the underestimation of POA by EMAC may be the treatment of wet deposition. The sensitivity of the results to the deposition parameterizations (e.g., the Henry's law constants for the organic vapors) will be tested in a subsequent article in preparation.

According to recent studies (Cappa and Wilson, 2012; Aumont et al., 2012; Zhang et al., 2013), not all oxidation products of SVOCs and IVOCs can be assigned to the OOA mass fraction since they are not sufficiently oxidized. Fountoukis et al. (2014) assumed that 50% of the simulated SOA-sv and SOA-iv is still considered as HOA by the AMS analysis and found significant improvements in the view of the modeled bias for POA. In this study we tested this hypothesis and we considered as POA the sum of fPOA and bbPOA and the 50% of the SOA-sv and SOA-iv produced from the first oxidation step of SVOCs and IVOCs, respectively. We assumed that SOA-sv and SOA-iv produced during any subsequent oxidation steps together with all the SOA-v are sufficiently oxidized to be considered 100% OOA. Following this hypothesis the model performance improved during winter (NME=55% μg m^{-3} and NMB=-28%) and autumn (NME=50% μg m^{-3} and NMB=1%) and reduced during spring (NME=110% μg m^{-3} and NMB=49%) and summer (NME=71% μg m^{-3} and NMB=16%) when the oxidation of SVOCs and IVOCs is enhanced significantly.

5.2.2 SOA

Atmos. Chem. Phys. Discuss., doi:10.5194/acp-2015-989, 2016
Manuscript under review for journal Atmos. Chem. Phys.
Published: 3 February 2016

Atmospheric Chemistry and Physics Discussions

The best performance of the model occurs during spring (NME=46%, NMB=-24%) followed by the autumn (NME=52%, NMB=-25%) and summer (NME=44%, NMB=-28%) (Table 3; Figure 11b). However, during winter the model strongly underpredicts OOA concentrations (NME=80%, NMB=-80%). The overall underprediction of OOA concentrations indicates that the model is missing an important source or formation pathway of SOA. Possible underestimation of residential biofuel emissions in our model, identified during the spatial and seasonal evaluation of simulated POA, can lead to an underestimation of SOA formed from the oxidation of these emissions during winter. Fountoukis et al. (2015) also reported low modeled SOA values compared to AMS OOA over the Paris region and attributed this discrepancy to the transformation of BBOA to OOA without the presence of sunlight reported by some recent studies (Bougiatioti et al., 2014; Crippa et al., 2013). Underestimation of cold-start vehicle emissions during winter can also lead to a significant underestimation of SOA since SOA produced from organic compounds emitted during the warm-up phase are 3-7 times higher than SOA produced when the catalyst is hot (Gordon et al., 2014). Furthermore, ORACLE assumes that the only source of SOA is the homogeneous gas-phase photochemical oxidation of SOA precursors. Therefore, the negative bias of the model could also be explained by its inability to simulate SOA formed from aqueous-phase and other heterogeneous reactions, including processes like oligomerization. Finally, the underprediction of SOA by the model during winter may be also associated with an overestimation of atmospheric removal.

PMF and EMAC results indicate that aged SOA levels exceed those of fresh SOA during all seasons. The EMAC performance for aged SOA appears to be better during spring (NMB=-33%), summer (NMB=-36%), and autumn (NMB=-32%), and much worse during winter (NMB=-91%) (Table 4; Figure 11c). The overall performance of the model for fresh SOA (NME=60%, NMB=-30%) (Table 5, Figure 11d) appears to be better than aged SOA (NME=71%, NMB=-40%) which supports our conclusions from the spatial model evaluation that the atmospheric aging of SOA may be underestimated by EMAC. However, this apparent discrepancy may be partially due to our assumption that LV-OOA corresponds only to multiple generational SOA. This hypothesis is not consistent with recent studies that reported formation of LV-OOA from the first oxidation step of biogenic VOCs (Ehn et al., 2014). During winter,

Atmos. Chem. Phys. Discuss., doi:10.5194/acp-2015-989, 2016
Manuscript under review for journal Atmos. Chem. Phys.
Published: 3 February 2016

EMAC also underestimates the fresh SOA levels (NMB=-79%). This underprediction of both fresh and aged SOA during winter suggests that one or more important wintertime SOA formation pathways are missing from our model.

5.3 OA composition

According to PMF results, the OOA/OA ratio increases downwind of the urban centers and in rural areas (from 61% over urban environments to 86% over remote areas; Figure 12a). This is in general consistent with the EMAC predictions. The predicted SOA/OA increases downwind of the urban centers (from 76% over urban locations to 80% over rural areas). This change is lower than the PMF estimates but could be explained by the uncertainty of the PMF analyses (Figure 12a). Alternatively, this may indicate that EMAC tends to underpredict the aging rate of OA. OOA/OA is consistently high during all seasons (around 80%) with the highest ratio predicted in summer (90%) and the lowest in winter (74%) (Figure 12b). The model predicts high SOA/OA during all seasons except winter (Figure 12b). The highest SOA/OA ratio is predicted during summer (87%) when the photo-oxidation of SOA is enhanced. The low SOA/OA during winter (47%) once again shows the inability of EMAC model to reproduce the observed SOA levels during that season.

Both PMF and EMAC indicate that aged SOA is higher than fresh SOA over all types of environment and seasons (Figure 13). PMF results suggest that LV-OOA/OOA is higher over urban-downwind environments (69%), while EMAC aged SOA/SOA is similar over all types of locations (59%) (Figure 13a). The high fresh SOA fraction estimated over rural areas by both PMF and EMAC (around 40%) indicates that fresh SOA production occurs even far away from the sources. The composition of OOA exhibits a seasonal cycle as well since AMS results indicate that LV-OOA/OOA is higher during winter (73%) and lower during summer (57%) (Figure 13b). EMAC predicts the highest aged SOA/SOA during spring (68%) and the lowest during winter (53%) without any clear seasonal pattern (Figure 13b).

6. Conclusions

This study estimates the impact of open biomass burning and anthropogenic combustion emissions (from fossil and biofuels) of SVOCs and IVOCs to global OA budgets and distributions. The EMAC simulations indicate that the tropospheric

burden of OA consists of 32% fOA and 30% bbOA. Furthermore, 90% of fOA and 70% of bbOA is predicted to be secondary. These results support recent findings from global studies that have also reported strong contributions of SOA from anthropogenic sources to global OA concentrations (Spracklen et al., 2011; Carslaw et al., 2013; Lee et al., 2013; Tsimpidi et al., 2014).

The tropospheric burdens of fOA and bbOA follow a clear seasonal pattern. fOA is higher during the boreal summer (0.63 Tg) and lower during winter (0.57 Tg), while bbOA is higher during the dry season in the tropics (1.15 Tg during August) and lower during the wet season (0.17 Tg during April). The simulated spatial distribution of fOA and bbOA is driven by the sources of their precursors and the range of their atmospheric transport. Higher fPOA concentrations occur over densely populated and highly industrialized areas of the Northern Hemisphere while further downwind fPOA decreases substantially due to dilution and evaporation. On the other hand, fSOA remains at high levels downwind of the anthropogenic sources due to the continued chemical transformations. bbPOA concentrations peak over the tropical and the boreal forests while bbSOA has high concentrations over a wide area covering most of South America, Central and South Africa, Southeastern Asia, Indonesia and even parts of the Southern Atlantic Ocean.

AMS results from 84 field campaigns performed in the Northern Hemisphere during the examined period (2001-2010) are also used to provide further insights into the composition of OA in three different types of environments: urban, urban-downwind and rural areas, during the four seasons of the year. The spatial analysis of AMS and EMAC results indicate that over urban areas POA is highest while further downwind and in rural areas decreases substantially due to dilution and evaporation. On the other hand, SOA is found to be high over all types of environments. This results in an increase of the SOA/OA ratio downwind of the urban centers. The seasonal analysis of the results performed in this study does not include the values over the urban areas since the model cannot reproduce the high OA concentrations over urban environments due to its limited spatial resolution. The seasonal evaluation of the model results against the AMS identified a major weakness of the model associated with its failure to reproduce the POA and SOA concentration levels during winter. This indicates that the model is probably missing both an important source and a formation pathway of OA, which becomes increasingly important during boreal

winter. Possible causes include the underestimation of residential biofuel emissions during winter, the underestimation of vehicle cold-start emissions, the neglect of aqueous-phase and heterogeneous oxidation reactions in the model, and the overestimation of the atmospheric removal of POA and freshly formed SOA.

AMS results indicate that OA consists of 15% HOA and 85% OOA on average during all four seasons. EMAC is able to reproduce this dominance of OOA and its results suggest that SOA accounts for 80% of total OA. At many locations, PMF analysis identified two subtypes of OOA that differ in volatility and oxidation state (LV-OOA and SV-OOA). PMF results indicate that LV-OOA is higher than SV-OOA regardless of the season or the type of environment. The overall LV-OOA/OOA during the four seasons of the year is 63% according to AMS measurement analysis. Assuming that SV-OOA corresponds to fresh SOA (first generation oxidation products) and LV-OOA corresponds to aged SOA (later generation oxidation products), EMAC is able to reproduce the PMF results predicting a dominance of aged SOA during all seasons (59% of the total SOA on average).

7. Acknowledgements

The research leading to these results has received funding from the European Research Council under the European Union's Seventh Framework Programme (FP7/2007-2013) / ERC grant agreement n° 226144. A.P. Tsimpidi acknowledges support from a DFG individual grand programme (project reference TS 335/2-1) and V.A. Karydis acknowledges support from a FP7 Marie Curie Career Integration Grant (project reference 618349).

8. References

Alvarado, M. J., Lonsdale, C. R., Yokelson, R. J., Akagi, S. K., Coe, H., Craven, J. S., Fischer, E. V., McMeeking, G. R., Seinfeld, J. H., Soni, T., Taylor, J. W., Weise, D. R., and Wold, C. E.: Investigating the links between ozone and organic aerosol chemistry in a biomass burning plume from a prescribed fire in California chaparral, Atmos. Chem. Phys., 15, 6667-6688, 10.5194/acp-15-6667-2015, 2015.

Aiken, A. C., Decarlo, P. F., Kroll, J. H., Worsnop, D. R., Huffman, J. A., Docherty, K. S., Ulbrich, I. M., Mohr, C., Kimmel, J. R., Sueper, D., Sun, Y., Zhang, Q., Trimborn, A., Northway, M., Ziemann, P. J., Canagaratna, M. R., Onasch, T. B., Alfarra, M. R., Prevot, A. S. H., Dommen, J., Duplissy, J., Metzger, A., Baltensperger, U., and Jimenez, J. L.: O/C and OM/OC ratios of primary, secondary, and ambient organic aerosols with high-resolution time-of-flight aerosol mass spectrometry, Environmen. Sci. & Technol., 42, 4478-4485, 2008.

734 Aiken, A. C., Salcedo, D., Cubison, M. J., Huffman, J. A., DeCarlo, P. F., Ulbrich, I.
735 M., Docherty, K. S., Sueper, D., Kimmel, J. R., Worsnop, D. R., Trimborn, A.,
736 Northway, M., Stone, E. A., Schauer, J. J., Volkamer, R. M., Fortner, E., de
737 Foy, B., Wang, J., Laskin, A., Shutthanandan, V., Zheng, J., Zhang, R.,
738 Gaffney, J., Marley, N. A., Paredes-Miranda, G., Arnott, W. P., Molina, L. T.,
739 Sosa, G., and Jimenez, J. L.: Mexico City aerosol analysis during MILAGRO
740 using high resolution aerosol mass spectrometry at the urban supersite (T0) -
741 Part 1: Fine particle composition and organic source apportionment, Atmo.
742 Chem. Phys., 9, 6633-6653, 2009.
743 Aiken, A. C., de Foy, B., Wiedinmyer, C., DeCarlo, P. F., Ulbrich, I. M., Wehrli, M.
744 N., Szidat, S., Prevot, A. S. H., Noda, J., Wacker, L., Volkamer, R., Fortner, E.,
745 Wang, J., Laskin, A., Shutthanandan, V., Zheng, J., Zhang, R., Paredes-
746 Miranda, G., Arnott, W. P., Molina, L. T., Sosa, G., Querol, X., and Jimenez, J.
747 L.: Mexico city aerosol analysis during MILAGRO using high resolution
748 aerosol mass spectrometry at the urban supersite (T0) - Part 2: Analysis of the
749 biomass burning contribution and the non-fossil carbon fraction, Atmo. Chem.
750 Phys., 10, 2010.
751 Allan, J. D., Alfarra, M. R., Bower, K. N., Williams, P. I., Gallagher, M. W., Jimenez,
752 J. L., McDonald, A. G., Nemitz, E., Canagaratna, M. R., Jayne, J. T., Coe, H.,
753 and Worsnop, D. R.: Quantitative sampling using an Aerodyne aerosol mass
754 spectrometer - 2. Measurements of fine particulate chemical composition in two
755 U.K. cities, J. Geophy. Res. Atmo., 108, doi: 10.1029/2002jd002359, 2003.
756 Athanasopoulou, E., Vogel, H., Vogel, B., Tsimpidi, A. P., Pandis, S. N., Knote, C.,
757 and Fountoukis, C.: Modeling the meteorological and chemical effects of
758 secondary organic aerosols during an EUCAARI campaign, Atmos. Chem.
759 Phys., 13, 625-645, 2013.
760 Aumont, B., Valorso, R., Mouchel-Vallon, C., Camredon, M., Lee-Taylor, J., and
761 Madronich, S.: Modeling SOA formation from the oxidation of intermediate
762 volatility n-alkanes, Atmo. Chem. Phys., 12, 7577-7589, 2012.
763 Bahreini, R., Middlebrook, A. M., de Gouw, J. A., Warneke, C., Trainer, M., Brock,
764 C. A., Stark, H., Brown, S. S., Dube, W. P., Gilman, J. B., Hall, K., Holloway,
765 J. S., Kuster, W. C., Perring, A. E., Prevot, A. S. H., Schwarz, J. P., Spackman,
766 J. R., Szidat, S., Wagner, N. L., Weber, R. J., Zotter, P., and Parrish, D. D.:
767 Gasoline emissions dominate over diesel in formation of secondary organic
768 aerosol mass, Geophys. Res. Lett., 39, doi: 10.1029/2011gl050718, 2012.
769 Bergstrom, R., van der Gon, H. A. C. D., Prevot, A. S. H., Yttri, K. E., and Simpson,
770 D.: Modelling of organic aerosols over Europe (2002-2007) using a volatility
771 basis set (VBS) framework: application of different assumptions regarding the
772 formation of secondary organic aerosol, Atmos. Chem. Phys., 12, 8499-8527,
773 2012.
774 Bond, T. C., Anderson, T. L., and Campbell, D.: Calibration and intercomparison of
775 filter-based measurements of visible light absorption by aerosols, Aerosol Sci.
776 Tech., 30, 582-600, 1999.
777 Bond, T. C.: Spectral dependence of visible light absorption by carbonaceous particles
778 emitted from coal combustion, Geophys. Res. Lett., 28, 4075-4078, doi:
779 10.1029/2001gl013652, 2001.
780 Bond, T. C., Streets, D. G., Yarber, K. F., Nelson, S. M., Woo, J. H., and Klimont, Z.:
781 A technology-based global inventory of black and organic carbon emissions

782 from combustion, J. Geophy. Res. Atmo., 109, doi: 10.1029/2003jd003697,
783 2004.
784 Bougiatioti, A., Stavroulas, I., Kostenidou, E., Zarmpas, P., Theodosi, C., Kouvarakis,
785 G., Canonaco, F., Prevot, A. S. H., Nenes, A., Pandis, S. N., and Mihalopoulos,
786 N.: Processing of biomass-burning aerosol in the eastern Mediterranean during
787 summertime, Atmo. Chem. Phys., 14, 4793-4807, 2014.
788 Cappa, C. D., and Wilson, K. R.: Multi-generation gas-phase oxidation, equilibrium
789 partitioning, and the formation and evolution of secondary organic aerosol,
790 Atmo. Chem. Phys., 12, 9505-9528, 2012.
791 Carbone, S., Aurela, M., Saarnio, K., Saarikoski, S., Timonen, H., Frey, A., Sueper,
792 D., Ulbrich, I. M., Jimenez, J. L., Kulmala, M., Worsnop, D. R., and Hillamo,
793 R. E.: Wintertime Aerosol Chemistry in Sub-Arctic Urban Air, Aerosol Sci.
794 Tech., 48, 313-323, 2014.
795 Carslaw, K. S., Lee, L. A., Reddington, C. L., Mann, G. W., and Pringle, K. J.: The
796 magnitude and sources of uncertainty in global aerosol, Faraday Discuss., 165,
797 495-512, 2013.
798 Chen, L. W. A., Watson, J. G., Chow, J. C., and Magliano, K. L.: Quantifying PM2.5
799 source contributions for the San Joaquin Valley with multivariate receptor
800 models, Environ. Sci. Tech., 41, 2818-2826, 2007.
801 Chen, Q., Farmer, D. K., Rizzo, L. V., Pauliquevis, T., Kuwata, M., Karl, T. G.,
802 Guenther, A., Allan, J. D., Coe, H., Andreae, M. O., Poschl, U., Jimenez, J. L.,
803 Artaxo, P., and Martin, S. T.: Submicron particle mass concentrations and
804 sources in the Amazonian wet season (AMAZE-08), Atmo. Chem. Phys., 15,
805 3687-3701, 2015.
806 Chen, Y., Morton, D. C., Jin, Y., Gollatz, G. J., Kasibhatla, P. S., van der Werf, G. R.,
807 DeFries, R. S., and Randerson, J. T.: Long-term trends and interannual
808 variability of forest, savanna and agricultural fires in South America, Carbon
809 Management, 4, 617-638, 2013.
810 Chirico, R., DeCarlo, P. F., Heringa, M. F., Tritscher, T., Richter, R., Prevot, A. S. H.,
811 Dommen, J., Weingartner, E., Wehrle, G., Gysel, M., Laborde, M., and
812 Baltensperger, U.: Impact of aftertreatment devices on primary emissions and
813 secondary organic aerosol formation potential from in-use diesel vehicles:
814 results from smog chamber experiments, Atmo. Chem. Phys., 10, 11545-11563,
815 2010.
816 Clarke, L., Edmonds, J., Jacoby, H., Pitcher, H., Reilly, J., and Richels, R.: Scenarios
817 of greenhouse gas emissions and atmospheric concentrations (Part A) and
818 review of integrated scenario development and application (Part B). A report by
819 the U.S. climate change science program and the subcommittee on global
820 change research, 2007.
821 Crippa, M., DeCarlo, P. F., Slowik, J. G., Mohr, C., Heringa, M. F., Chirico, R.,
822 Poulain, L., Freutel, F., Sciare, J., Cozic, J., Di Marco, C. F., Elsasser, M.,
823 Nicolas, J. B., Marchand, N., Abidi, E., Wiedensohler, A., Drewnick, F.,
824 Schneider, J., Borrmann, S., Nemitz, E., Zimmermann, R., Jaffrezo, J. L.,
825 Prevot, A. S. H., and Baltensperger, U.: Wintertime aerosol chemical
826 composition and source apportionment of the organic fraction in the
827 metropolitan area of Paris, Atmo. Chem. Phys., 13, 961-981, 2013.
828 Crippa, M., Canonaco, F., Lanz, V. A., Aijala, M., Allan, J. D., Carbone, S., Capes,
829 G., Ceburnis, D., Dall'Osto, M., Day, D. A., DeCarlo, P. F., Ehn, M., Eriksson,
830 A., Freney, E., Ruiz, L. H., Hillamo, R., Jimenez, J. L., Junninen, H., Kiendler-

Scharr, A., Kortelainen, A. M., Kulmala, M., Laaksonen, A., Mensah, A., Mohr, C., Nemitz, E., O'Dowd, C., Ovadnevaite, J., Pandis, S. N., Petaja, T., Poulain, L., Saarikoski, S., Sellegri, K., Swietlicki, E., Tiitta, P., Worsnop, D. R., Baltensperger, U., and Prevot, A. S. H.: Organic aerosol components derived from 25 AMS data sets across Europe using a consistent ME-2 based source apportionment approach, Atmo. Chem. Phys., 14, 2014.

de Gouw, J. A., Middlebrook, A. M., Warneke, C., Goldan, P. D., Kuster, W. C., Roberts, J. M., Fehsenfeld, F. C., Worsnop, D. R., Canagaratna, M. R., Pszenny, A. A. P., Keene, W. C., Marchewka, M., Bertman, S. B., and Bates, T. S.: Budget of organic carbon in a polluted atmosphere: Results from the New England Air Quality Study in 2002, J. Geophy. Res. Atmo., 110, doi: 10.1029/2004jd005623, 2005.

DeCarlo, P. F., Ulbrich, I. M., Crounse, J., de Foy, B., Dunlea, E. J., Aiken, A. C., Knapp, D., Weinheimer, A. J., Campos, T., Wennberg, P. O., and Jimenez, J. L.: Investigation of the sources and processing of organic aerosol over the Central Mexican Plateau from aircraft measurements during MILAGRO, Atmo. Chem. Phys., 10, 5257-5280, 2010.

Denier van der Gon, H. A. C., Bergström, R., Fountoukis, C., Johansson, C., Pandis, S. N., Simpson, D., and Visschedijk, A.: Particulate emissions from residential wood combustion in Europe – revised estimates and an evaluation, Atmos. Chem. Phys. Discuss., 14, 31719-31765, 2014.

Donahue, N. M., Robinson, A. L., Stanier, C. O., and Pandis, S. N.: Coupled partitioning, dilution, and chemical aging of semivolatile organics, Environ. Sci. Technol., 40, 2635-2643, 2006.

Donahue, N. M., Robinson, A. L., and Pandis, S. N.: Atmospheric organic particulate matter: From smoke to secondary organic aerosol, Atmo. Environ., 43, 94-106, 2009.

Ehn, M., Thornton, J. A., Kleist, E., Sipila, M., Junninen, H., Pullinen, I., Springer, M., Rubach, F., Tillmann, R., Lee, B., Lopez-Hilfiker, F., Andres, S., Acir, I.-H., Rissanen, M., Jokinen, T., Schobesberger, S., Kangasluoma, J., Kontkanen, J., Nieminen, T., Kurten, T., Nielsen, L. B., Jorgensen, S., Kjaergaard, H. G., Canagaratna, M., Maso, M. D., Berndt, T., Petaja, T., Wahner, A., Kerminen, V.-M., Kulmala, M., Worsnop, D. R., Wildt, J., and Mentel, T. F.: A large source of low-volatility secondary organic aerosol, Nature, 506, doi: 10.1038/nature13032, 2014.

Fountoukis, C., Racherla, P. N., van der Gon, H. A. C. D., Polymeneas, P., Charalampidis, P. E., Pilinis, C., Wiedensohler, A., Dall'Osto, M., O'Dowd, C., and Pandis, S. N.: Evaluation of a three-dimensional chemical transport model (PMCAMx) in the European domain during the EUCAARI May 2008 campaign, Atmos. Chem. and Phys., 11, 10331-10347, 2011.

Fountoukis, C., Megaritis, A. G., Skyllakou, K., Charalampidis, P. E., Pilinis, C., van der Gon, H., Crippa, M., Canonaco, F., Mohr, C., Prevot, A. S. H., Allan, J. D., Poulain, L., Petaja, T., Tiitta, P., Carbone, S., Kiendler-Scharr, A., Nemitz, E., O'Dowd, C., Swietlicki, E., and Pandis, S. N.: Organic aerosol concentration and composition over Europe: insights from comparison of regional model predictions with aerosol mass spectrometer factor analysis, Atmo. Chem. Phys., 14, 9061-9076, 2014.

Fountoukis, C., Megaritis, A. G., Skyllakou, K., Charalampidis, P. E., Denier van der Gon, H. A. C., Crippa, M., Prévôt, A. S. H., Freutel, F., Wiedensohler, A.,

880 Pilinis, C., and Pandis, S. N.: Simulating the formation of carbonaceous aerosol
881 in a European Megacity (Paris) during the MEGAPOLI summer and winter
882 campaigns, Atmos. Chem. Phys. Discuss., 15, 25547-25582, 2015.
883 Gentner, D. R., Isaacman, G., Worton, D. R., Chan, A. W. H., Dallmann, T. R., Davis,
884 L., Liu, S., Day, D. A., Russell, L. M., Wilson, K. R., Weber, R., Guha, A.,
885 Harley, R. A., and Goldstein, A. H.: Elucidating secondary organic aerosol from
886 diesel and gasoline vehicles through detailed characterization of organic carbon
887 emissions, Proceedings of the National Academy of Sciences of the United
888 States of America, 109, 18318-18323, 2012.
889 Goldstein, A. H., and Galbally, I. E.: Known and unexplored organic constituents in
890 the earth's atmosphere, Environ. Sci. Tech., 41, 1514-1521, 2007.
891 Gordon, T. D., Presto, A. A., May, A. A., Nguyen, N. T., Lipsky, E. M., Donahue, N.
892 M., Gutierrez, A., Zhang, M., Maddox, C., Rieger, P., Chattopadhyay, S.,
893 Maldonado, H., Maricq, M. M., and Robinson, A. L.: Secondary organic aerosol
894 formation exceeds primary particulate matter emissions for light-duty gasoline
895 vehicles, Atmo. Chem. Phys., 14, 2014.
896 Grieshop, A. P., Logue, J. M., Donahue, N. M., and Robinson, A. L.: Laboratory
897 investigation of photochemical oxidation of organic aerosol from wood fires 1:
898 measurement and simulation of organic aerosol evolution, Atmos. Chem. Phys.,
899 9, 1263-1277, 2009.
900 Hayes, P. L., Ortega, A. M., Cubison, M. J., Froyd, K. D., Zhao, Y., Cliff, S. S., Hu,
901 W. W., Toohey, D. W., Flynn, J. H., Lefer, B. L., Grossberg, N., Alvarez, S.,
902 Rappenglueck, B., Taylor, J. W., Allan, J. D., Holloway, J. S., Gilman, J. B.,
903 Kuster, W. C., De Gouw, J. A., Massoli, P., Zhang, X., Liu, J., Weber, R. J.,
904 Corrigan, A. L., Russell, L. M., Isaacman, G., Worton, D. R., Kreisberg, N. M.,
905 Goldstein, A. H., Thalman, R., Waxman, E. M., Volkamer, R., Lin, Y. H.,
906 Surratt, J. D., Kleindienst, T. E., Offenberg, J. H., Dusanter, S., Griffith, S.,
907 Stevens, P. S., Brioude, J., Angevine, W. M., and Jimenez, J. L.: Organic
908 aerosol composition and sources in Pasadena, California, during the 2010
909 CalNex campaign, J. Geophy. Res. Atmo., 118, 9233-9257, doi:
910 10.1002/jgrd.50530, 2013.
911 Heald, C. L., Jacob, D. J., Park, R. J., Russell, L. M., Huebert, B. J., Seinfeld, J. H.,
912 Liao, H., and Weber, R. J.: A large organic aerosol source in the free
913 troposphere missing from current models, Geophys. Res. Lett., 32, doi:
914 10.1029/2005gl023831, 2005.
915 Henze, D. K., Seinfeld, J. H., Ng, N. L., Kroll, J. H., Fu, T. M., Jacob, D. J., and
916 Heald, C. L.: Global modeling of secondary organic aerosol formation from
917 aromatic hydrocarbons: high- vs. low-yield pathways, Atmo. Chem. Phys., 8,
918 2405-2420, 2008.
919 Herndon, S. C., Onasch, T. B., Wood, E. C., Kroll, J. H., Canagaratna, M. R., Jayne,
920 J. T., Zavala, M. A., Knighton, W. B., Mazzoleni, C., Dubey, M. K., Ulbrich, I.
921 M., Jimenez, J. L., Seila, R., de Gouw, J. A., de Foy, B., Fast, J., Molina, L. T.,
922 Kolb, C. E., and Worsnop, D. R.: Correlation of secondary organic aerosol with
923 odd oxygen in Mexico City, Geophys. Res. Lett., 35, doi:
924 10.1029/2008gl034058, 2008.
925 Hildemann, L. M., Cass, G. R., and Markowski, G. R.: A dilution stack sampler for
926 collection of organic aerosol emissions-Desigh, characterization and filed-tests,
927 Aerosol Sci. Tech., 10, 193-204, 1989.

928 Hodzic, A., Jimenez, J. L., Madronich, S., Canagaratna, M. R., DeCarlo, P. F.,
929 Kleinman, L., and Fast, J.: Modeling organic aerosols in a megacity: potential
930 contribution of semi-volatile and intermediate volatility primary organic
931 compounds to secondary organic aerosol formation, Atmos. Chem. Phys., 10,
932 5491-5514, 2010.
933 Jacobson, M. Z.: Isolating nitrated and aromatic aerosols and nitrated aromatic gases
934 as sources of ultraviolet light absorption, J. Geophy. Res. Atmo., 104, 3527-
935 3542, doi: 10.1029/1998jd100054, 1999.
936 Jathar, S. H., Farina, S. C., Robinson, A. L., and Adams, P. J.: The influence of semi-
937 volatile and reactive primary emissions on the abundance and properties of
938 global organic aerosol, Atmos. Chem. Phys., 11, 7727-7746, 2011.
939 Jayne, J. T., Leard, D. C., Zhang, X. F., Davidovits, P., Smith, K. A., Kolb, C. E., and
940 Worsnop, D. R.: Development of an aerosol mass spectrometer for size and
941 composition analysis of submicron particles, Aerosol Sci. Tech., 33, 49-70,
942 2000.
943 Jimenez, J. L., Jayne, J. T., Shi, Q., Kolb, C. E., Worsnop, D. R., Yourshaw, I.,
944 Seinfeld, J. H., Flagan, R. C., Zhang, X. F., Smith, K. A., Morris, J. W., and
945 Davidovits, P.: Ambient aerosol sampling using the Aerodyne Aerosol Mass
946 Spectrometer, J. Geophy. Res. Atmo., 108, doi: 10.1029/2001jd001213, 2003.
947 Jimenez, J. L., Canagaratna, M. R., Donahue, N. M., Prevot, A. S. H., Zhang, Q.,
948 Kroll, J. H., DeCarlo, P. F., Allan, J. D., Coe, H., Ng, N. L., Aiken, A. C.,
949 Docherty, K. S., Ulbrich, I. M., Grieshop, A. P., Robinson, A. L., Duplissy, J.,
950 Smith, J. D., Wilson, K. R., Lanz, V. A., Hueglin, C., Sun, Y. L., Tian, J.,
951 Laaksonen, A., Raatikainen, T., Rautiainen, J., Vaattovaara, P., Ehn, M.,
952 Kulmala, M., Tomlinson, J. M., Collins, D. R., Cubison, M. J., Dunlea, E. J.,
953 Huffman, J. A., Onasch, T. B., Alfarra, M. R., Williams, P. I., Bower, K.,
954 Kondo, Y., Schneider, J., Drewnick, F., Borrmann, S., Weimer, S., Demerjian,
955 K., Salcedo, D., Cottrell, L., Griffin, R., Takami, A., Miyoshi, T., Hatakeyama,
956 S., Shimono, A., Sun, J. Y., Zhang, Y. M., Dzepina, K., Kimmel, J. R., Sueper,
957 D., Jayne, J. T., Herndon, S. C., Trimborn, A. M., Williams, L. R., Wood, E. C.,
958 Middlebrook, A. M., Kolb, C. E., Baltensperger, U., and Worsnop, D. R.:
959 Evolution of organic aerosols in the atmosphere, Science, 326, 1525-1529,
960 2009.
961 Jöckel, P., Tost, H., Pozzer, A., Bruehl, C., Buchholz, J., Ganzeveld, L., Hoor, P.,
962 Kerkweg, A., Lawrence, M. G., Sander, R., Steil, B., Stiller, G., Tanarhte, M.,
963 Taraborrelli, D., Van Aardenne, J., and Lelieveld, J.: The atmospheric chemistry
964 general circulation model ECHAM5/MESSy1: consistent simulation of ozone
965 from the surface to the mesosphere, Atmos. Chem. Phys., 6, 5067-5104, 2006.
966 Kanakidou, M., Seinfeld, J. H., Pandis, S. N., Barnes, I., Dentener, F. J., Facchini, M.
967 C., Van Dingenen, R., Ervens, B., Nenes, A., Nielsen, C. J., Swietlicki, E.,
968 Putaud, J. P., Balkanski, Y., Fuzzi, S., Horth, J., Moortgat, G. K., Winterhalter,
969 R., Myhre, C. E. L., Tsigaridis, K., Vignati, E., Stephanou, E. G., and Wilson,
970 J.: Organic aerosol and global climate modelling: a review, Atmos. Chem.
971 Phys., 5, 1053-1123, 2005.
972 Kerkweg, A., Buchholz, J., Ganzeveld, L., Pozzer, A., Tost, H., and Jöckel, P.:
973 Technical Note: An implementation of the dry removal processes DRY
974 DEPosition and SEDImentation in the Modular Earth Submodel System
975 (MESSy), Atmos. Chem. Phys., 6, 4617-4632, 2006a.

976 Kerkweg, A., Sander, R., Tost, H., and Jöckel, P.: Technical note: Implementation of
977 prescribed (OFFLEM), calculated (ONLEM), and pseudo-emissions
978 (TNUDGE) of chemical species in the Modular Earth Submodel System
979 (MESSy), Atmos. Chem. Phys., 6, 3603-3609, 2006b.
980 Kirchstetter, T. W., Novakov, T., and Hobbs, P. V.: Evidence that the spectral
981 dependence of light absorption by aerosols is affected by organic carbon, J.
982 Geophy. Res. Atmo., 109, doi: 10.1029/2004jd004999, 2004.
983 Kopacz, M., Jacob, D. J., Fisher, J. A., Logan, J. A., Zhang, L., Megretskaia, I. A.,
984 Yantosca, R. M., Singh, K., Henze, D. K., Burrows, J. P., Buchwitz, M.,
985 Khlystova, I., McMillan, W. W., Gille, J. C., Edwards, D. P., Eldering, A.,
986 Thouret, V., and Nedelec, P.: Global estimates of CO sources with high
987 resolution by adjoint inversion of multiple satellite datasets (MOPITT, AIRS,
988 SCIAMACHY, TES), Atmos. Chem. Phys., 10, 855-876, 10.5194/acp-10-855-
989 2010, 2010.
990 Kostenidou, E., Kaltsonoudis, C., Tsiflikiotou, M., Louvaris, E., Russell, L. M., and
991 Pandis, S. N.: Burning of olive tree branches: a major organic aerosol source in
992 the Mediterranean, Atmo. Chem. Phys., 13, 8797-8811, 2013.
993 Kotchenruther, R. A., and Hobbs, P. V.: Humidification factors of aerosols from
994 biomass burning in Brazil, J. Geophy. Res. Atmo., 103, 32081-32089, doi:
995 10.1029/98jd00340, 1998.
996 Kotchenruther, R. A., Hobbs, P. V., and Hegg, D. A.: Humidification factors for
997 atmospheric aerosols off the mid-Atlantic coast of the United States, J. Geophy.
998 Res. Atmo., 104, 2239-2251, doi: 10.1029/98jd01751, 1999.
999 Kroll, J. H., and Seinfeld, J. H.: Chemistry of secondary organic aerosol: Formation
1000 and evolution of low-volatility organics in the atmosphere, Atmos. Environ., 42,
1001 3593-3624, 2008.
1002 Lanz, V. A., Alfarra, M. R., Baltensperger, U., Buchmann, B., Hueglin, C., and
1003 Prevot, A. S. H.: Source apportionment of submicron organic aerosols at an
1004 urban site by factor analytical modelling of aerosol mass spectra, Atmo. Chem.
1005 Phys., 7, 1503-1522, 2007.
1006 Lanz, V. A., Alfarra, M. R., Baltensperger, U., Buchmann, B., Hueglin, C., Szidat, S.,
1007 Wehrli, M. N., Wacker, L., Weimer, S., Caseiro, A., Puxbaum, H., and Prevot,
1008 A. S. H.: Source attribution of submicron organic aerosols during wintertime
1009 inversions by advanced factor analysis of aerosol mass spectra, Environ. Sci.
1010 Tech., 42, 214-220, 2008.
1011 Lanz, V. A., Prevot, A. S. H., Alfarra, M. R., Weimer, S., Mohr, C., DeCarlo, P. F.,
1012 Gianini, M. F. D., Hueglin, C., Schneider, J., Favez, O., D'Anna, B., George, C.,
1013 and Baltensperger, U.: Characterization of aerosol chemical composition with
1014 aerosol mass spectrometry in Central Europe: an overview, Atmo. Chem. Phys.,
1015 10, 10453-10471, 2010.
1016 Lauer, A., Eyring, V., Hendricks, J., Joeckel, P., and Lohmann, U.: Global model
1017 simulations of the impact of ocean-going ships on aerosols, clouds, and the
1018 radiation budget, Atmos. Chem. Phys., 7, 5061-5079, 2007.
1019 Lee, L. A., Pringle, K. J., Reddington, C. L., Mann, G. W., Stier, P., Spracklen, D. V.,
1020 Pierce, J. R., and Carslaw, K. S.: The magnitude and causes of uncertainty in
1021 global model simulations of cloud condensation nuclei, Atmos. Chem. Phys.,
1022 13, 8879-8914, 2013.

1023 Lelieveld, J., Barlas, C., Giannadaki, D., and Pozzer, A.: Model calculated global,
1024 regional and megacity premature mortality due to air pollution, Atmo. Chem.
1025 Phys., 13, 7023-7037, 2013.
1026 Lipsky, E. M., and Robinson, A. L.: Effects of dilution on fine particle mass and
1027 partitioning of semivolatile organics in diesel exhaust and wood smoke,
1028 Environ. Sci. Technol., 40, 155-162, 2006.
1029 Marcolli, C., Canagaratna, M. R., Worsnop, D. R., Bahreini, R., de Gouw, J. A.,
1030 Warneke, C., Goldan, P. D., Kuster, W. C., Williams, E. J., Lerner, B. M.,
1031 Roberts, J. M., Meagher, J. F., Fehsenfeld, F. C., Marchewka, M., Bertman, S.
1032 B., and Middlebrook, A. M.: Cluster analysis of the organic peaks in bulk mass
1033 spectra obtained during the 2002 New England air quality study with an
1034 Aerodyne aerosol mass spectrometer, Atmo. Chem. Phys., 6, 5649-5666, 2006.
1035 May, A. A., Levin, E. J. T., Hennigan, C. J., Riipinen, I., Lee, T., Collett, J. L.,
1036 Jimenez, J. L., Kreidenweis, S. M., and Robinson, A. L.: Gas-particle
1037 partitioning of primary organic aerosol emissions: 3. Biomass burning, J.
1038 Geophy. Res. Atmo., 118, 11327-11338, doi: 10.1002/jgrd.50828, 2013.
1039 McFiggans, G., Artaxo, P., Baltensperger, U., Coe, H., Facchini, M. C., Feingold, G.,
1040 Fuzzi, S., Gysel, M., Laaksonen, A., Lohmann, U., Mentel, T. F., Murphy, D.
1041 M., O'Dowd, C. D., Snider, J. R., and Weingartner, E.: The effect of physical
1042 and chemical aerosol properties on warm cloud droplet activation, Atmo. Chem.
1043 Phys., 6, 2593-2649, 2006.
1044 McKeown, P. J., Johnston, M. V., and Murphy, D. M.: Online single-particle analysis
1045 by laser desorption mass-spectrometry, Anal. Chem., 63, 2069-2073, 1991.
1046 Miracolo, M. A., Hennigan, C. J., Ranjan, M., Nguyen, N. T., Gordon, T. D., Lipsky,
1047 E. M., Presto, A. A., Donahue, N. M., and Robinson, A. L.: Secondary aerosol
1048 formation from photochemical aging of aircraft exhaust in a smog chamber,
1049 Atmo. Chem. Phys., 11, 4135-4147, 2011.
1050 Mohr, C., DeCarlo, P. F., Heringa, M. F., Chirico, R., Slowik, J. G., Richter, R.,
1051 Reche, C., Alastuey, A., Querol, X., Seco, R., Penuelas, J., Jimenez, J. L.,
1052 Crippa, M., Zimmermann, R., Baltensperger, U., and Prevot, A. S. H.:
1053 Identification and quantification of organic aerosol from cooking and other
1054 sources in Barcelona using aerosol mass spectrometer data, Atmo. Chem. Phys.,
1055 12, 1649-1665, 2012.
1056 Murphy, B. N., and Pandis, S. N.: Simulating the formation of semivolatile primary
1057 and secondary organic aerosol in a regional chemical transport model, Environ.
1058 Sci. Technol., 43, 4722-4728, 2009.
1059 Nemitz, E., Jimenez, J. L., Huffman, J. A., Ulbrich, I. M., Canagaratna, M. R.,
1060 Worsnop, D. R., and Guenther, A. B.: An eddy-covariance system for the
1061 measurement of surface/atmosphere exchange fluxes of submicron aerosol
1062 chemical species - First application above an urban area, Aerosol Sci. Tech., 42,
1063 636-657, 2008.
1064 Ng, N. L., Canagaratna, M. R., Jimenez, J. L., Zhang, Q., Ulbrich, I. M., and
1065 Worsnop, D. R.: Real-Time Methods for Estimating Organic Component Mass
1066 Concentrations from Aerosol Mass Spectrometer Data, Environ. Sci. Tech., 45,
1067 910-916, 2011.
1068 Paatero, P., and Tapper, U.: Positive matrix factorization-A nonnegative factor model
1069 with optimal utilization of error-estimates of data values, Environmetrics, 5,
1070 111-126, 1994.

1071 Paatero, P.: Least squares formulation of robust non-negative factor analysis,
1072 Chemometrics and Intelligent Laboratory Systems, 37, 23-35, 1997.
1073 Poschl, U.: Atmospheric aerosols: Composition, transformation, climate and health
1074 effects, Angew. Chem.-Int. Edit., 44, 7520-7540, 2005.
1075 Pringle, K. J., Tost, H., Message, S., Steil, B., Giannadaki, D., Nenes, A., Fountoukis,
1076 C., Stier, P., Vignati, E., and Leieved, J.: Description and evaluation of GMXe:
1077 a new aerosol submodel for global simulations (v1), Geoscientific Model
1078 Development, 3, 391-412, 2010.
1079 Pye, H. O. T., and Seinfeld, J. H.: A global perspective on aerosol from low-volatility
1080 organic compounds, Atmos. Chem. Phys., 10, 4377-4401, 2010.
1081 Robinson, A. L., Donahue, N. M., Shrivastava, M. K., Weitkamp, E. A., Sage, A. M.,
1082 Grieshop, A. P., Lane, T. E., Pierce, J. R., and Pandis, S. N.: Rethinking organic
1083 aerosols: Semivolatile emissions and photochemical aging, Science, 315, 1259-
1084 1262, 2007.
1085 Robinson, A. L., Grieshop, A. P., Donahue, N. M., and Hunt, S. W.: Updating the
1086 conceptual model for fine particle mass emissions from combustion systems, J.
1087 Air Waste Manage., 60, 1204-1222, 2010.
1088 Samy, S., and Zielinska, B.: Secondary organic aerosol production from modern
1089 diesel engine emissions, Atmo. Chem. Phys., 10, 609-625, 2010.
1090 Sander, R., Baumgaertner, A., Gromov, S., Harder, H., Joeckel, P., Kerkweg, A.,
1091 Kubistin, D., Regelin, E., Riede, H., Sandu, A., Taraborrelli, D., Tost, H., and
1092 Xie, Z. Q.: The atmospheric chemistry box model CAABA/MECCA-3.0,
1093 Geoscientific Model Development, 4, 373-380, 2011.
1094 Schauer, J. J., Kleeman, M. J., Cass, G. R., and Simoneit, B. R. T.: Measurement of
1095 emissions from air pollution sources. 2. C-1 through C-30 organic compounds
1096 from medium duty diesel trucks, Environ. Sci. Technol., 33, 1578-1587, 1999.
1097 Schauer, J. J., Kleeman, M. J., Cass, G. R., and Simoneit, B. R. T.: Measurement of
1098 emissions from air pollution sources. 3. C-1-C-29 organic compounds from
1099 fireplace combustion of wood, Environ. Sci. Technol., 35, 1716-1728, 2001.
1100 Schauer, J. J., Kleeman, M. J., Cass, G. R., and Simoneit, B. R. T.: Measurement of
1101 emissions from air pollution sources. 5. C-1-C-32 organic compounds from
1102 gasoline-powered motor vehicles, Environ. Sci. Technol., 36, 1169-1180, 2002.
1103 Shrivastava, M. K., Lane, T. E., Donahue, N. M., Pandis, S. N., and Robinson, A. L.:
1104 Effects of gas particle partitioning and aging of primary emissions on urban and
1105 regional organic aerosol concentrations, J. Geophys. Res. Atmos., 113, doi:
1106 10.1029/2007jd009735, 2008.
1107 Spracklen, D. V., Jimenez, J. L., Carslaw, K. S., Worsnop, D. R., Evans, M. J., Mann,
1108 G. W., Zhang, Q., Canagaratna, M. R., Allan, J., Coe, H., McFiggans, G., Rap,
1109 A., and Forster, P.: Aerosol mass spectrometer constraint on the global
1110 secondary organic aerosol budget, Atmo. Chem. Phys., 11, 12109-12136, 2011.
1111 Stone, E. A., Zhou, J., Snyder, D. C., Rutter, A. P., Mieritz, M., and Schauer, J. J.: A
1112 Comparison of Summertime Secondary Organic Aerosol Source Contributions
1113 at Contrasting Urban Locations, Environ. Sci. Tech., 43, 3448-3454, 2009.
1114 Subramanian, R., Donahue, N. M., Bernardo-Bricker, A., Rogge, W. F., and
1115 Robinson, A. L.: Insights into the primary-secondary and regional-local
1116 contributions to organic aerosol and PM2.5 mass in Pittsburgh, Pennsylvania,
1117 Atmo. Environ., 41, 7414-7433, 2007.
1118 Suess, D. T., and Prather, K. A.: Mass spectrometry of aerosols, Chemical Reviews,
1119 99, 3007-+, 1999.

1120 Takegawa, N., Miyazaki, Y., Kondo, Y., Komazaki, Y., Miyakawa, T., Jimenez, J. L.,
1121 Jayne, J. T., Worsnop, D. R., Allan, J. D., and Weber, R. J.: Characterization of
1122 an Aerodyne Aerosol Mass Spectrometer (AMS): Intercomparison with other
1123 aerosol instruments, Aerosol Sci. Tech., 39, 760-770, 2005.
1124 Tsigaridis, K., Daskalakis, N., Kanakidou, M., Adams, P. J., Artaxo, P., Bahadur, R.,
1125 Balkanski, Y., Bauer, S. E., Bellouin, N., Benedetti, A., Bergman, T., Berntsen,
1126 T. K., Beukes, J. P., Bian, H., Carslaw, K. S., Chin, M., Curci, G., Diehl, T.,
1127 Easter, R. C., Ghan, S. J., Gong, S. L., Hodzic, A., Hoyle, C. R., Iversen, T.,
1128 Jathar, S., Jimenez, J. L., Kaiser, J. W., Kirkevag, A., Koch, D., Kokkola, H.,
1129 Lee, Y. H., Lin, G., Liu, X., Luo, G., Ma, X., Mann, G. W., Mihalopoulos, N.,
1130 Morcrette, J. J., Mueller, J. F., Myhre, G., Myriokefalitakis, S., Ng, N. L.,
1131 O'Donnell, D., Penner, J. E., Pozzoli, L., Pringle, K. J., Russell, L. M., Schulz,
1132 M., Sciare, J., Seland, O., Shindell, D. T., Sillman, S., Skeie, R. B., Spracklen,
1133 D., Stavrakou, T., Steenrod, S. D., Takemura, T., Tiitta, P., Tilmes, S., Tost, H.,
1134 van Noije, T., van Zyl, P. G., von Salzen, K., Yu, F., Wang, Z., Wang, Z.,
1135 Zaveri, R. A., Zhang, H., Zhang, K., Zhang, Q., and Zhang, X.: The AeroCom
1136 evaluation and intercomparison of organic aerosol in global models, Atmo.
1137 Chem. Phys., 14, 10845-10895, 2014.
1138 Tsimpidi, A. P., Karydis, V. A., Zavala, M., Lei, W., Molina, L., Ulbrich, I. M.,
1139 Jimenez, J. L., and Pandis, S. N.: Evaluation of the volatility basis-set approach
1140 for the simulation of organic aerosol formation in the Mexico City metropolitan
1141 area, Atmos. Chem. Phys., 10, 525-546, 2010.
1142 Tsimpidi, A. P., Karydis, V. A., Zavala, M., Lei, W., Bei, N., Molina, L., and Pandis,
1143 S. N.: Sources and production of organic aerosol in Mexico City: insights from
1144 the combination of a chemical transport model (PMCAMx-2008) and
1145 measurements during MILAGRO, Atmos. Chem. Phys., 11, 5153-5168, 2011.
1146 Tsimpidi, A. P., Karydis, V. A., Pozzer, A., Pandis, S. N., and Lelieveld, J.: ORACLE
1147 (v1.0): module to simulate the organic aerosol composition and evolution in the
1148 atmosphere, Geoscientific Model Development, 7, 3153-3172, 2014.
1149 Turpin, B. J., Saxena, P., and Andrews, E.: Measuring and simulating particulate
1150 organics in the atmosphere: problems and prospects, Atmo. Environ., 34, 2983-
1151 3013, 2000.
1152 Ulbrich, I. M., Canagaratna, M. R., Zhang, Q., Worsnop, D. R., and Jimenez, J. L.:
1153 Interpretation of organic components from Positive Matrix Factorization of
1154 aerosol mass spectrometric data, Atmo. Chem. Phys., 9, 2891-2918, 2009.
1155 van der Werf, G. R., Randerson, J. T., Giglio, L., Collatz, G. J., Mu, M., Kasibhatla,
1156 P. S., Morton, D. C., DeFries, R. S., Jin, Y., and van Leeuwen, T. T.: Global fire
1157 emissions and the contribution of deforestation, savanna, forest, agricultural,
1158 and peat fires (1997-2009), Atmos. Chem. Phys., 10, 11707-11735, 2010.
1159 Volkamer, R., Jimenez, J. L., San Martini, F., Dzepina, K., Zhang, Q., Salcedo, D.,
1160 Molina, L. T., Worsnop, D. R., and Molina, M. J.: Secondary organic aerosol
1161 formation from anthropogenic air pollution: Rapid and higher than expected,
1162 Geophys. Res. Lett., 33, doi: 10.1029/2006gl026899, 2006.
1163 Vutukuru, S., Griffin, R. J., and Dabdub, D.: Simulation and analysis of secondary
1164 organic aerosol dynamics in the South Coast Air Basin of California, J. Geophy.
1165 Res. Atmo., 111, doi: 10.1029/2005jd006139, 2006.
1166 Wang, Q., Shao, M., Liu, Y., William, K., Paul, G., Li, X., Liu, Y., and Lu, S.: Impact
1167 of biomass burning on urban air quality estimated by organic tracers:

1168 Guangzhou and Beijing as cases, Atmo. Environ., 41, 8380-8390, doi:
1169 10.1016/j.atmosenv.2007.06.048, 2007.
1170 Weilenmann, M., Favez, J.-Y., and Alvarez, R.: Cold-start emissions of modern
1171 passenger cars at different low ambient temperatures and their evolution over
1172 vehicle legislation categories, Atmos. Environ., 43, 2419-2429, 2009.
1173 Weitkamp, E. A., Sage, A. M., Pierce, J. R., Donahue, N. M., and Robinson, A. L.:
1174 Organic aerosol formation from photochemical oxidation of diesel exhaust in a
1175 smog chamber, Environ. Sci. Tech., 41, 6969-6975, 2007.
1176 Westerholm, R., Christensen, A., and Rosen, A.: Regulated and unregulated exhaust
1177 emissions from two three-way catalyst equipped gasoline fuelled vehicles,
1178 Atmos. Environ., 30, 3529-3536, 1996.
1179 Zhang, Q., Alfarra, M. R., Worsnop, D. R., Allan, J. D., Coe, H., Canagaratna, M. R.,
1180 and Jimenez, J. L.: Deconvolution and quantification of hydrocarbon-like and
1181 oxygenated organic aerosols based on aerosol mass spectrometry, Environ. Sci.
1182 Tech., 39, 4938-4952, 2005a.
1183 Zhang, Q., Canagaratna, M. R., Jayne, J. T., Worsnop, D. R., and Jimenez, J. L.:
1184 Time- and size-resolved chemical composition of submicron particles in
1185 Pittsburgh: Implications for aerosol sources and processes, J. Geophys. Res.-
1186 Atmos., 110, doi: 10.1029/2004jd004649, 2005b.
1187 Zhang, Q., Worsnop, D. R., Canagaratna, M. R., and Jimenez, J. L.: Hydrocarbon-like
1188 and oxygenated organic aerosols in Pittsburgh: insights into sources and
1189 processes of organic aerosols, Atmo. Chem. Phys., 5, 3289-3311, 2005c.
1190 Zhang, Q., Jimenez, J. L., Canagaratna, M. R., Allan, J. D., Coe, H., Ulbrich, I.,
1191 Alfarra, M. R., Takami, A., Middlebrook, A. M., Sun, Y. L., Dzepina, K.,
1192 Dunlea, E., Docherty, K., DeCarlo, P. F., Salcedo, D., Onasch, T., Jayne, J. T.,
1193 Miyoshi, T., Shimono, A., Hatakeyama, S., Takegawa, N., Kondo, Y.,
1194 Schneider, J., Drewnick, F., Borrmann, S., Weimer, S., Demerjian, K.,
1195 Williams, P., Bower, K., Bahreini, R., Cottrell, L., Griffin, R. J., Rautiainen, J.,
1196 Sun, J. Y., Zhang, Y. M., and Worsnop, D. R.: Ubiquity and dominance of
1197 oxygenated species in organic aerosols in anthropogenically-influenced
1198 Northern Hemisphere midlatitudes, Geophys. Res. Lett., 34, doi:
1199 10.1029/2007gl029979, 2007.
1200 Zhang, Q., Jimenez, J. L., Canagaratna, M. R., Ulbrich, I. M., Ng, N. L., Worsnop, D.
1201 R., and Sun, Y. L.: Understanding atmospheric organic aerosols via factor
1202 analysis of aerosol mass spectrometry: a review, Anal. Bioanal. Chem., 401,
1203 3045-3067, 2011.
1204 Zhang, Q. J., Beekmann, M., Drewnick, F., Freutel, F., Schneider, J., Crippa, M.,
1205 Prevot, A. S. H., Baltensperger, U., Poulain, L., Wiedensohler, A., Sciare, J.,
1206 Gros, V., Borbon, A., Colomb, A., Michoud, V., Doussin, J. F., van der Gon, H.
1207 A. C. D., Haeffelin, M., Dupont, J. C., Siour, G., Petetin, H., Bessagnet, B.,
1208 Pandis, S. N., Hodzic, A., Sanchez, O., Honore, C., and Perrussel, O.:
1209 Formation of organic aerosol in the Paris region during the MEGAPOLI
1210 summer campaign: evaluation of the volatility-basis-set approach within the
1211 CHIMERE model, Atmos. Chem. Phys., 13, 5767-5790, 2013.

1212

1213

1214

Atmos. Chem. Phys. Discuss., doi:10.5194/acp-2015-989, 2016
Manuscript under review for journal Atmos. Chem. Phys.
Published: 3 February 2016

Atmospheric Chemistry and Physics Discussions

1215

1216 **Table 1.** Predicted tropospheric burden in Tg of organic aerosol components during the
1217 decade 2001-2010.

OA component	**Tropospheric burden** (Tg)	**Monthly Standard Deviation** (σ)
fPOA	0.06	0.01
fSOA	0.57	0.06
bbPOA	0.18	0.13
bbSOA	0.41	0.27
OA	1.98	0.54

1218

Atmos. Chem. Phys. Discuss., doi:10.5194/acp-2015-989, 2016
Manuscript under review for journal Atmos. Chem. Phys.
Published: 3 February 2016

Atmospheric Chemistry and Physics Discussions

1219

1220 **Table 2.** Statistical evaluation of EMAC POA (sum of fPOA and bbPOA) against
1221 AMS POA (sum of HOA and BBOA) from 84 data sets worldwide during 2001-2010.
1222

Site Type[a]	**Number of datasets**	**Mean Observed** (μg m^{-3})	**Mean Predicted** (μg m^{-3})	**MAGE** (μg m^{-3})	**MB** (μg m^{-3})	**NME** (%)	**NMB** (%)	**RMSE** (μg m^{-3})
Urban	22	2.74	0.96	1.79	-1.79	65	-65	2.64
Urban Downwind	14	0.69	0.59	0.35	-0.10	51	-15	0.45
Rural/Remote	46	0.43	0.47	0.37	0.04	87	9	0.5
Season[b]								
Winter	5	0.93	0.61	0.51	-0.32	55	-34	0.69
Spring	31	0.44	0.53	0.41	0.09	94	21	0.52
Summer	13	0.45	0.44	0.30	-0.01	68	-3	0.40
Autumn	11	0.49	0.42	0.27	-0.07	54	-15	0.37
Total	60	0.49	0.50	0.37	0.01	75	1	0.49

1223 [a] Statistics are calculated for a specific site type during all four seasons
1224 [b] Statistics are calculated for a specific season excluding the values from urban areas
1225

Atmos. Chem. Phys. Discuss., doi:10.5194/acp-2015-989, 2016
Manuscript under review for journal Atmos. Chem. Phys.
Published: 3 February 2016

Atmospheric Chemistry and Physics Discussions

1226 **Table 3.** Statistical evaluation of EMAC SOA against AMS OOA from 84 data sets
1227 worldwide during 2001-2010.
1228

Site Type[a]	Number of datasets	Mean Observed (μg m^{-3})	Mean Predicted (μg m^{-3})	MAGE (μg m^{-3})	MB (μg m^{-3})	NME (%)	NMB (%)	RMSE (μg m^{-3})
Urban	22	4.33	2.97	1.96	-1.36	45	-31	2.51
Urban Downwind	14	2.95	2.20	1.07	-0.75	.36	-25	1.64
Rural/Remote	46	2.72	1.86	1.45	-0.86	54	-32	2.09
Season[b]								
Winter	5	2.72	0.55	2.17	-2.17	80	-80	2.56
Spring	31	2.38	1.80	1.10	-0.58	46	-24	1.47
Summer	13	4.07	2.94	1.81	-1.13	44	-28	3.01
Autumn	11	2.35	1.78	1.22	-0.57	52	-25	1.39
Total	60	2.77	1.94	1.36	-0.83	49	-30	2.00

1229 [a] Statistics are calculated for a specific site type during all four seasons
1230 [b] Statistics are calculated for a specific season excluding the values from urban areas
1231

Atmos. Chem. Phys. Discuss., doi:10.5194/acp-2015-989, 2016
Manuscript under review for journal Atmos. Chem. Phys.
Published: 3 February 2016

Atmospheric Chemistry and Physics Discussions

1232 **Table 4.** Statistical evaluation of EMAC aged SOA against AMS LV-OOA from 51
1233 data sets worldwide during 2001-2010.
1234

Site Type[a]	Number of datasets	Mean Observed (μg m^{-3})	Mean Predicted (μg m^{-3})	MAGE (μg m^{-3})	MB (μg m^{-3})	NME (%)	NMB (%)	RMSE (μg m^{-3})
Urban	10	3.43	2.72	1.47	-0.72	43	-21	2.04
Urban Downwind	8	1.77	0.94	1.28	-0.83	72	-47	1.55
Rural/Remote	33	1.65	1.02	1.17	-0.63	71	-38	1.69
Season[b]								
Winter	3	2.36	0.20	2.16	-2.16	91	-91	2.36
Spring	19	1.25	0.84	0.94	-0.41	76	-33	1.25
Summer	10	2.45	1.57	1.64	-0.88	67	-36	2.38
Autumn	9	1.49	1.01	0.89	-0.48	59	-32	1.10
Total	41	1.68	1.01	1.19	-0.67	71	-40	1.67

1235 [a] Statistics are calculated for a specific site type during all four seasons
1236 [b] Statistics are calculated for a specific season excluding the values from urban areas
1237

Atmos. Chem. Phys. Discuss., doi:10.5194/acp-2015-989, 2016
Manuscript under review for journal Atmos. Chem. Phys.
Published: 3 February 2016

Atmospheric Chemistry and Physics Discussions

1238 **Table 5.** Statistical evaluation of EMAC fresh SOA against AMS SV-OOA from 51
1239 data sets worldwide during 2001-2010.
1240

Site Type[a]	Number of datasets	Mean Observed (μg m^{-3})	Mean Predicted (μg m^{-3})	MAGE (μg m^{-3})	MB (μg m^{-3})	NME (%)	NMB (%)	RMSE (μg m^{-3})
Urban	10	2.14	1.88	0.69	-0.26	32	-12	0.81
Urban Downwind	8	0.81	0.64	0.41	-0.17	51	-21	0.76
Rural/Remote	33	1.03	0.70	0.64	-0.33	62	-32	0.85
Season[b]								
Winter	3	0.87	0.18	0.69	-0.69	79	-79	0.76
Spring	19	0.65	0.40	0.53	-0.25	81	-39	0.71
Summer	10	1.81	1.25	0.88	-0.56	48	-31	1.21
Autumn	9	0.83	0.86	0.39	0.03	47	4	0.52
Total	41	0.99	0.69	0.60	-0.30	60	-30	0.83

1241 [a] Statistics are calculated for a specific site type during all four seasons
1242 [b] Statistics are calculated for a specific season excluding the values from urban areas
1243
1244

Atmos. Chem. Phys. Discuss., doi:10.5194/acp-2015-989, 2016
Manuscript under review for journal Atmos. Chem. Phys.
Published: 3 February 2016

Atmospheric Chemistry and Physics Discussions

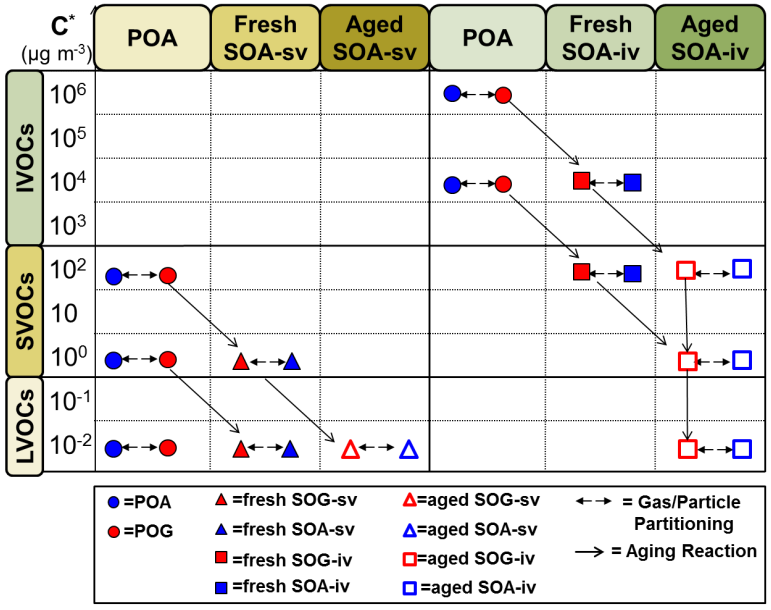

Figure 1: Schematic of the VBS resolution and the formation of SOA from SVOC and IVOC emissions. Red indicates the vapor phase and blue the particulate phase. The circles represent primary organic material that can be emitted either in the gas or in the aerosol phase. Filled triangles and squares indicate the formation of SOA from SVOCs and IVOCs, respectively, by fuel combustion and biomass burning sources from the first oxidation step (fresh SOA). Open triangles and squares represent SOA formed in additional oxidation steps (aged SOA) from SVOCs and IVOCs by the same sources. The partitioning processes, the aging reactions of the organic compounds, and the names of the species used to track all compounds are also shown.

Atmos. Chem. Phys. Discuss., doi:10.5194/acp-2015-989, 2016
Manuscript under review for journal Atmos. Chem. Phys.
Published: 3 February 2016

Atmospheric Chemistry and Physics Discussions

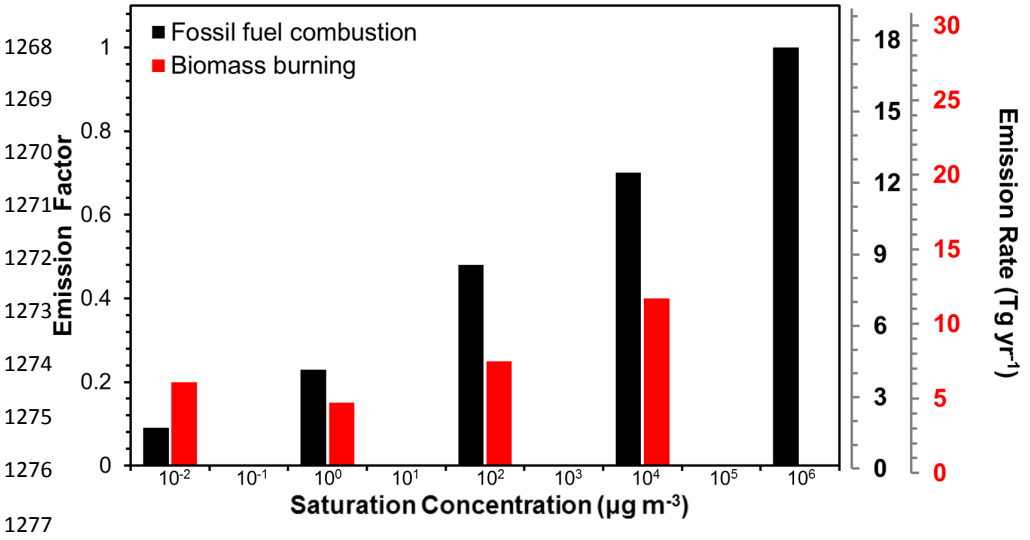

Figure 2. Volatility distribution for fuel combustion (in black) and biomass burning (in red) organic emissions. The emission factors for fuel combustion emissions are derived from Robinson et al. (2007) while for biomass burning POA emissions are from May et al. (2013) (shown in the primary y-axis). The corresponding emission rates are also shown in the secondary y-axis.

Atmos. Chem. Phys. Discuss., doi:10.5194/acp-2015-989, 2016
Manuscript under review for journal Atmos. Chem. Phys.
Published: 3 February 2016

Atmospheric Chemistry and Physics Discussions

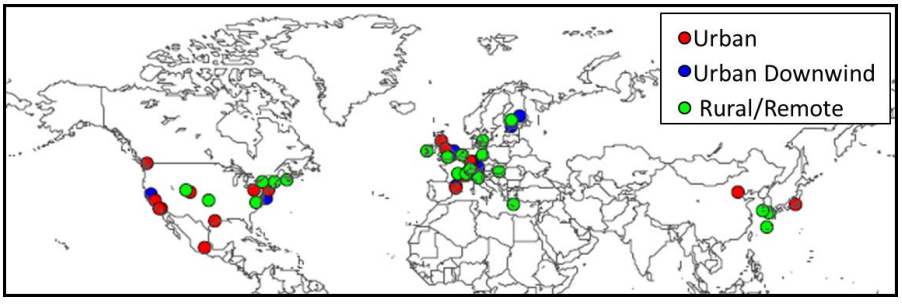

Figure 3: Location of the field measurement campaigns used for evaluating the model during 2001-2010. Urban, urban downwind and rural/remote areas are represented by red, blue, and green colors respectively.

Atmos. Chem. Phys. Discuss., doi:10.5194/acp-2015-989, 2016
Manuscript under review for journal Atmos. Chem. Phys.
Published: 3 February 2016

Atmospheric Chemistry and Physics Discussions

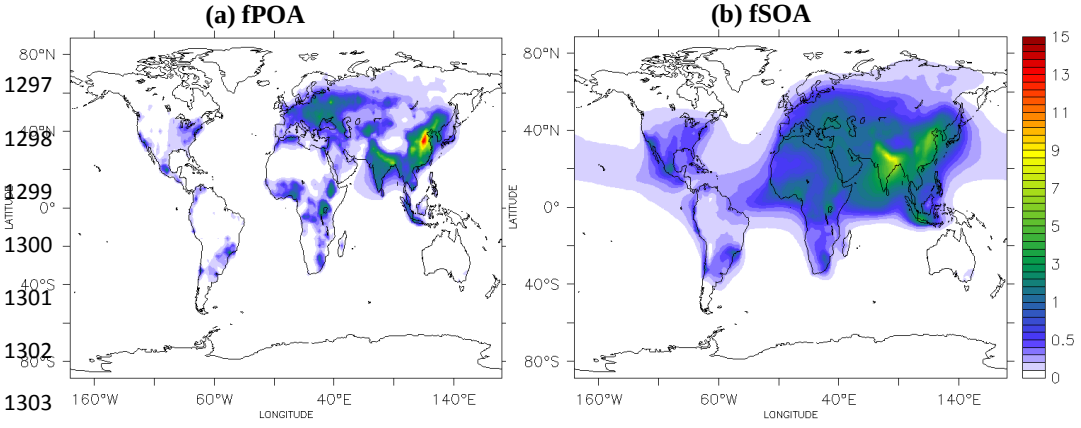

Figure 4: Predicted average surface concentrations (in μg m^{-3}) of: **(a)** POA from fuel combustion sources (fPOA) and **(b)** SOA from the oxidation of SVOCs and IVOCs from fuel combustion sources (fSOA) during the years 2001-2010.

Atmos. Chem. Phys. Discuss., doi:10.5194/acp-2015-989, 2016
Manuscript under review for journal Atmos. Chem. Phys.
Published: 3 February 2016

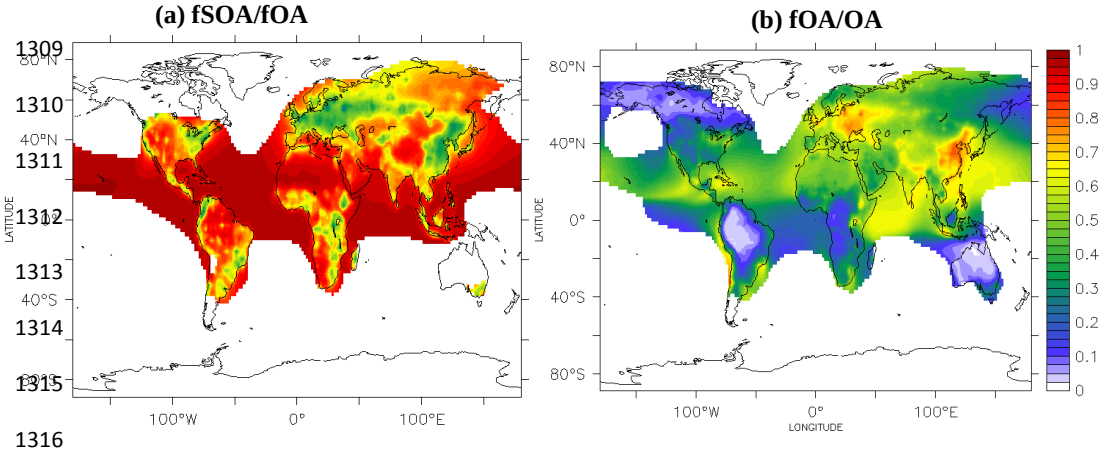

Figure 5: Predicted ratio of **(a)** fuel combustion SOA (fSOA) to total fuel combustion OA (sum of fPOA and fSOA) and **(b)** fuel combustion OA to total OA (sum of fOA, bbOA, aSOA, and bSOA) during the years 2001-2010.

Atmos. Chem. Phys. Discuss., doi:10.5194/acp-2015-989, 2016
Manuscript under review for journal Atmos. Chem. Phys.
Published: 3 February 2016

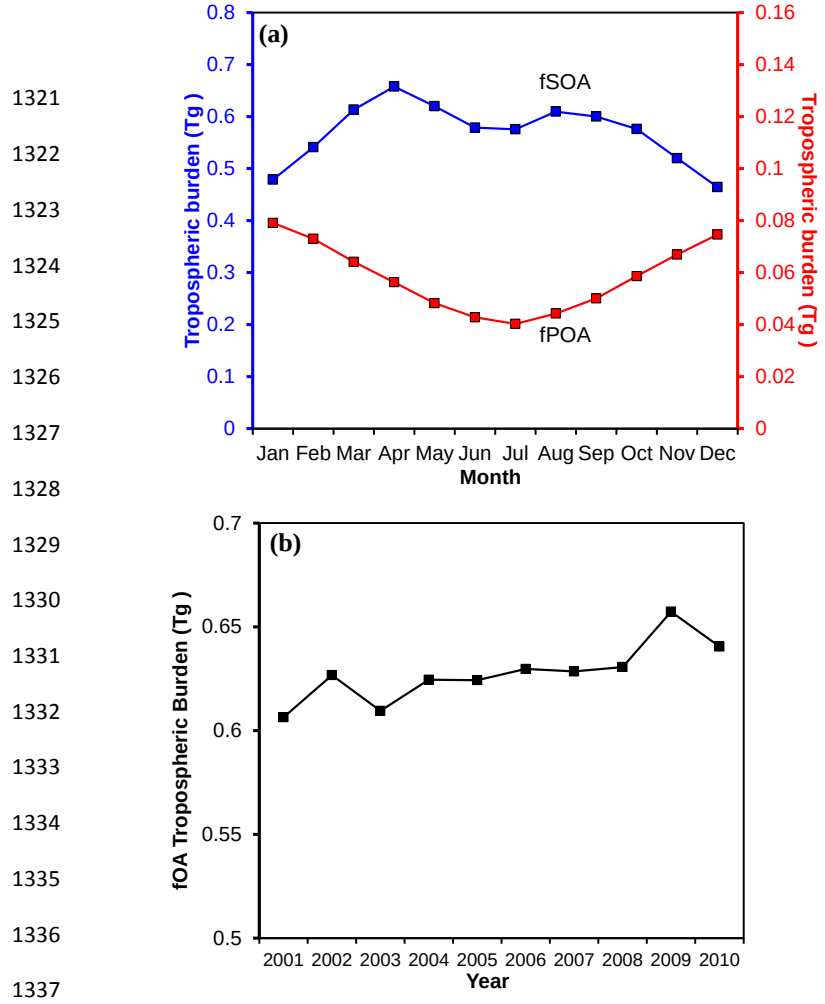

Figure 6: (a) Average predicted tropospheric burden (Tg) of fSOA (in blue, primary y-axis) and fPOA (in red, secondary y-axis) during the year and **(b)** annually averaged tropospheric burden of total fuel combustion OA (fOA) during 2001-2010.

Atmos. Chem. Phys. Discuss., doi:10.5194/acp-2015-989, 2016
Manuscript under review for journal Atmos. Chem. Phys.
Published: 3 February 2016

Atmospheric Chemistry and Physics Discussions

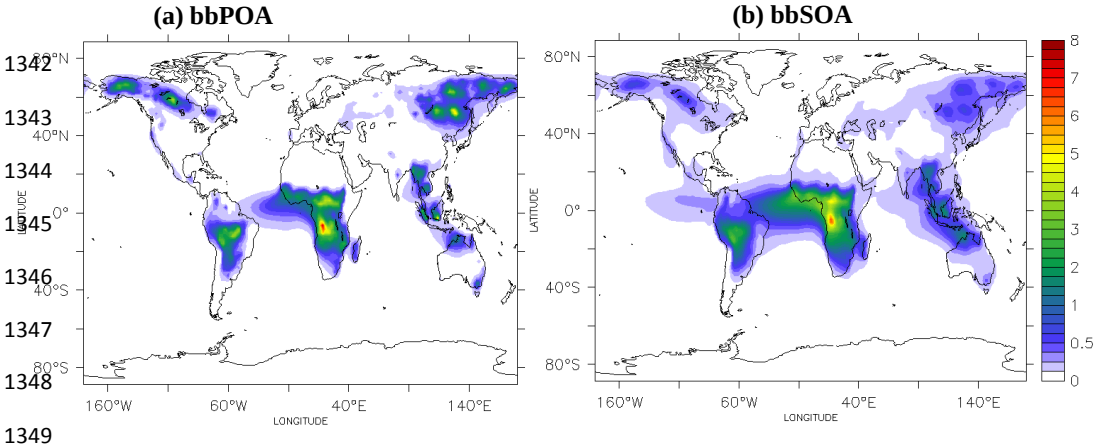

Figure 7: Predicted average surface concentrations (in μg m^{-3}) of: **(a)** POA from biomass burning sources (bbPOA) and **(b)** SOA from the oxidation of SVOCs and IVOCs from biomass burning sources (bbSOA) during the years 2001-2010.

Atmos. Chem. Phys. Discuss., doi:10.5194/acp-2015-989, 2016
Manuscript under review for journal Atmos. Chem. Phys.
Published: 3 February 2016

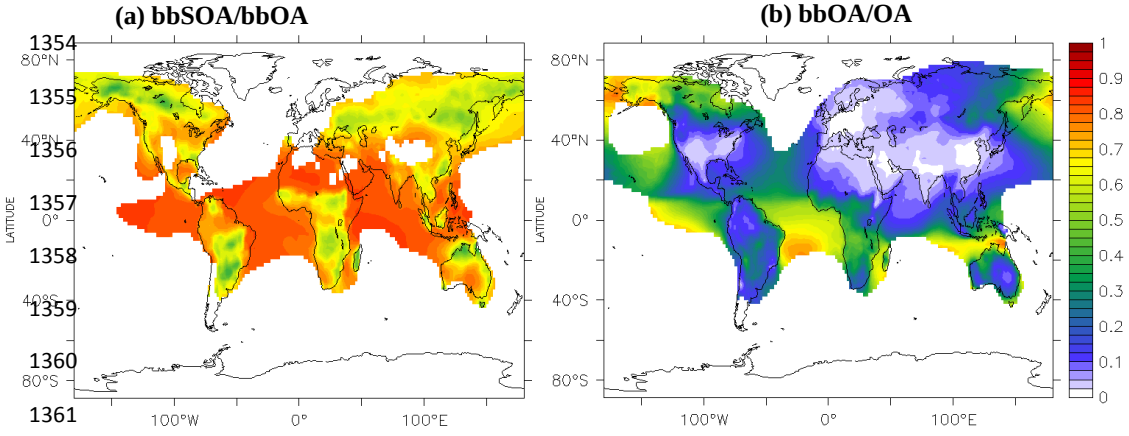

Figure 8: Predicted ratio of **(a)** biomass burning SOA (bbSOA) to total biomass burning OA (sum of bbPOA and bbSOA) and **(b)** biomass burning OA to total OA (sum of fOA, bbOA, aSOA, and bSOA) during the years 2001-2010.

Atmos. Chem. Phys. Discuss., doi:10.5194/acp-2015-989, 2016
Manuscript under review for journal Atmos. Chem. Phys.
Published: 3 February 2016

Atmospheric Chemistry and Physics Discussions

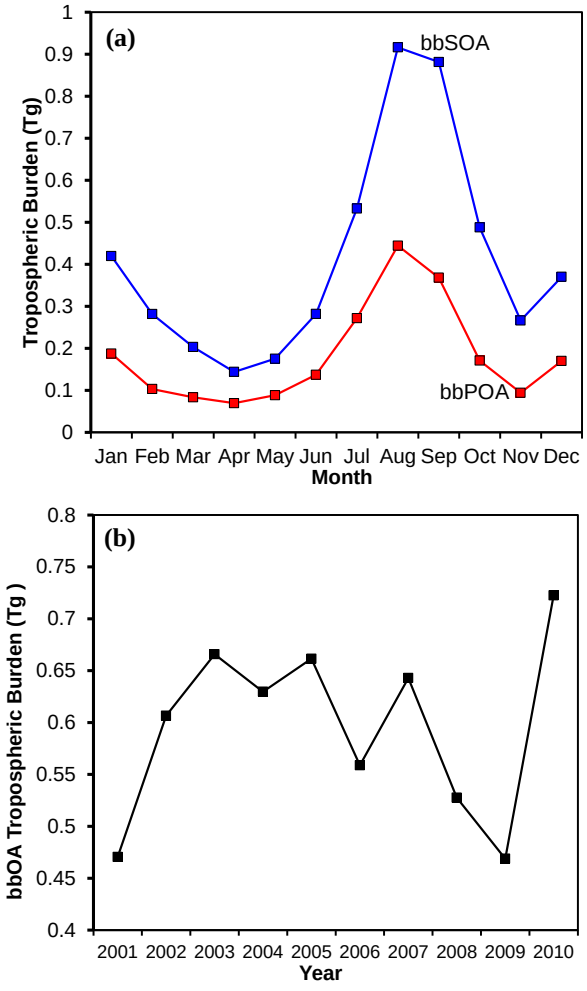

Figure 9: (a) Monthly averaged predicted tropospheric burden (Tg) of bbSOA (in blue) and bbPOA (in red) and **(b)** Annual average tropospheric burden of total biomass burning OA (bbOA) during 2001-2010.

Atmos. Chem. Phys. Discuss., doi:10.5194/acp-2015-989, 2016
Manuscript under review for journal Atmos. Chem. Phys.
Published: 3 February 2016

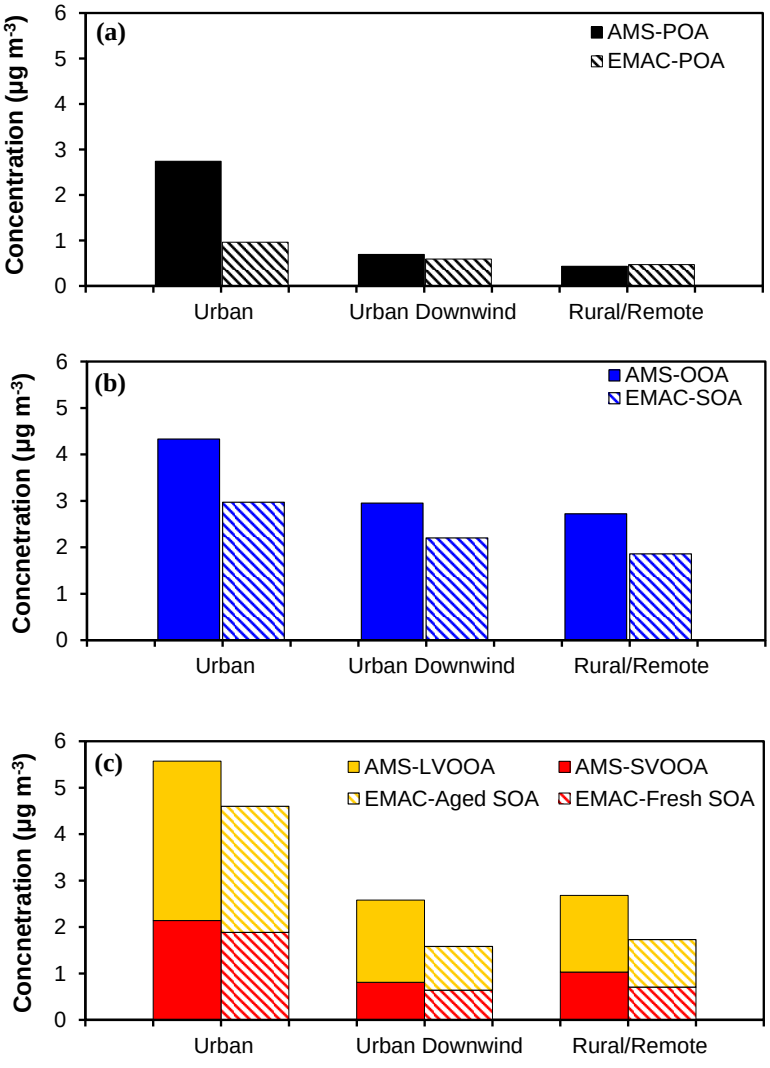

Figure 10: Comparison of average **(a)** predicted POA against AMS-POA (sum of AMS-HOA and AMS-BBOA) **(b)** predicted SOA against AMS-OOA, and, **(c)** predicted fresh SOA and aged SOA against AMS-SVOOA and AMS-LVOOA from 84 data sets worldwide over urban, urban downwind and rural/remote areas during 2001-2010.

Atmos. Chem. Phys. Discuss., doi:10.5194/acp-2015-989, 2016
Manuscript under review for journal Atmos. Chem. Phys.
Published: 3 February 2016

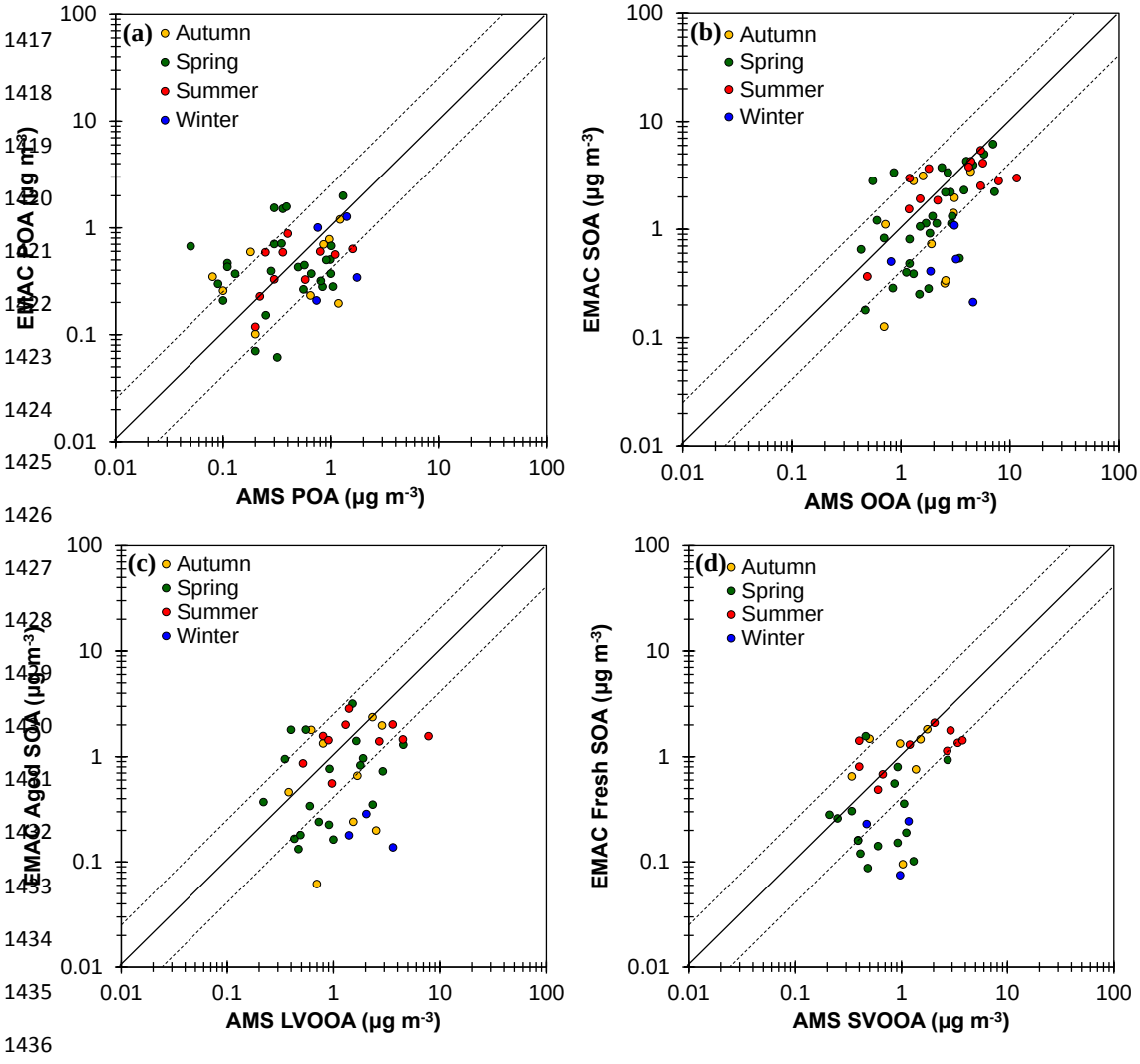

Figure 11: Scatterplots comparing model results against AMS for: **(a)** POA, **(b)** OOA, **(c)** LV-OOA, and **(d)** SV-OOA concentrations (in µg m^{-3}) derived from 84 data sets over the Northern Hemisphere during 2001-2010. Each point represents the data set average value and is colored based on the season the field campaign took place. Also shown are the 1:1, 2:1, and 1:2 lines.

Atmos. Chem. Phys. Discuss., doi:10.5194/acp-2015-989, 2016
Manuscript under review for journal Atmos. Chem. Phys.
Published: 3 February 2016

Atmospheric Chemistry and Physics Discussions

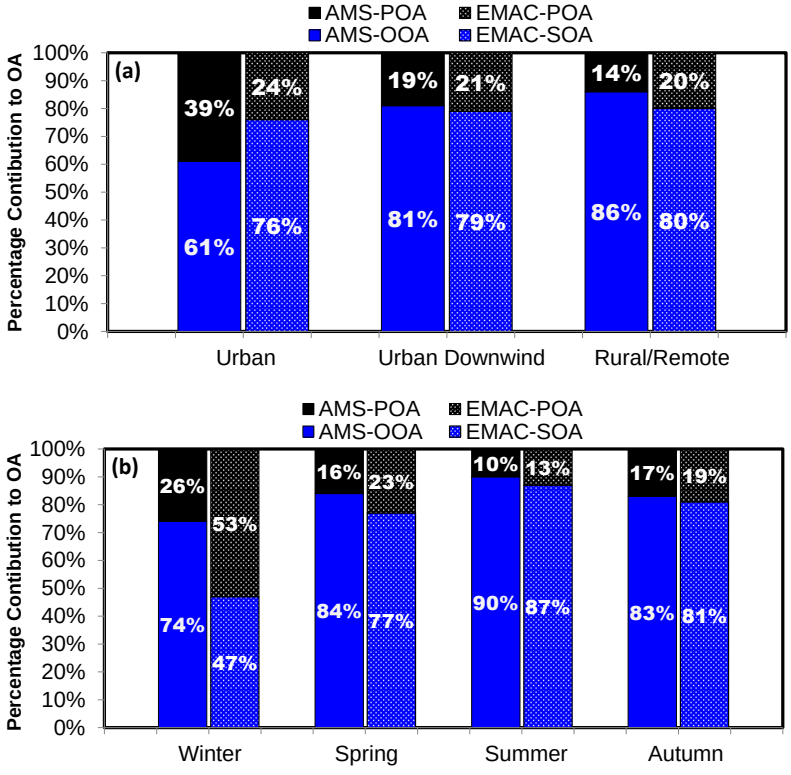

Figure 12: (a) Spatial and **(b)** seasonal composition of total OA mass calculated from EMAC and AMS results for 84 data sets worldwide during 2001-2010

Atmos. Chem. Phys. Discuss., doi:10.5194/acp-2015-989, 2016
Manuscript under review for journal Atmos. Chem. Phys.
Published: 3 February 2016

Atmospheric Chemistry and Physics Discussions

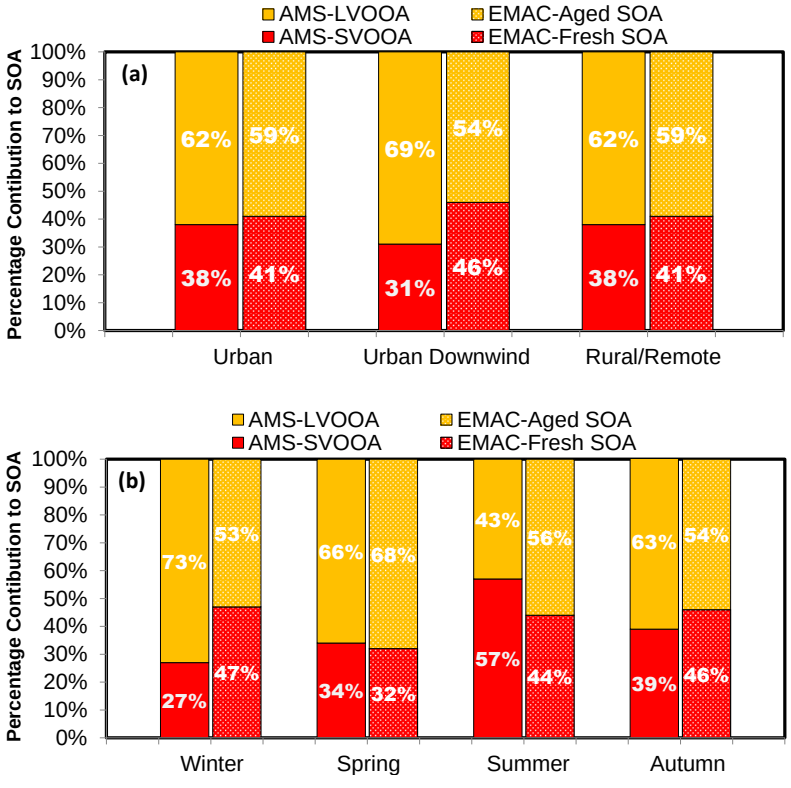

Figure 13: (a) Spatial and **(b)** seasonal composition of SOA and OOA mass calculated from EMAC and AMS results, respectively, for 51 data sets worldwide during 2001-2010